Investigation of Grouted Helical Pier based Foundation Rehabilitation -Centrifuge Data Report for YYB01

Yueying Bian[1], Tara C. Hutchinson[2], Dan Wilson[3] and Debra F. Laefer[4]

1. Department of Civil and Environmental Engineering, University of California, Irvine, USA
2. Department of Structural Engineering, University of California, San Diego, USA
3. Department of Civil & Environmental Engineering, University of California, Davis, USA
4. School of Architecture, Landscape & Civil Engineering, University College Dublin, Ireland

Date of report: November, 2007
Date of testing: June, 2006
Project: Investigation of grouted helical pier based foundation rehabilitation
NSF contract No.: CMS-0513972
Sponsor(s): U.S. National Science Foundation
Previous reports in this test series: None

ACKNOWLEDGEMENTS

The research project was funded by the U.S. National Science Foundation (NSF) under the direction of Dr. T.C. Hutchinson, Dr. D. Wilson and Dr. D.F. Laefer. Grouted materials were generously donated by Surecrete, Inc., DeNeef Construction Chemicals, and Concrete Technologies.

The tests were performed using the geotechnical centrifuge at the University of California, Davis. The authors acknowledge the technical assistance from Chad Justice, Tom Coker, Lars Pedersen and Bob Kazanjy at University of California, Davis and Irvine. Special thanks to Mr. Dean White of Concrete Technologies and Mr. Russell Lindsey of Precision Pier USA, Inc. Professors Scott, Brandenberg at University of California, Los Angeles and Bruce Kutter of UC Davis provided helpful suggestions and technical input. Professor Brandenberg provided the tomographic image data.

CONDITIONS AND LIMITATIONS

TABLE OF CONTENT

Page

LIST OF FIGURES

Page

LIST OF TABLES

Page

CHAPTER 1: PURPOSE AND GENERAL CONFIGURATION OF THE TEST

This data report describes the centrifuge test that was performed in June 2006 on the UC Davis geotechnical centrifuge. The purpose of the test was to develop the instruments and materials for in-flight grouting and simulate and study the working mechanisms and properties of *grouted helical pier systems* (GHPS). The testing procedures, methods, and observations during the testing series are described in this report. Prior to centrifuge testing, 1-g bucket tests were also performed to develop suitable materials and tools for the piers planned for placement in the centrifuge and these 1-g tests are also summarized in this report. Additional data analysis may be found in Bian (2006).

The soil used to construct the model was air pluviated #30 sand, which was obtained commercially from White Cap Construction Supply. A series of seven spin up and down cycles were performed to either grout or load the piers in flight. In total, one plain (non-grouted) pier, one helical (non-grouted) pier and 16 grouted helical piers were placed. The most important data from these experiments was post-test excavation observations.

General configuration parameters for the test are as follows:

Centrifuge:	9-m-radius centrifuge at UC Davis
Model Container:	Flexible Shear Beam (FSB-1) Soil Container
Centrifuge Acceleration:	15-g

The centrifuge allows modeling of prototype soil stresses and thus captures the strength and deformation characteristics of the soil. A model specimen subjected to N-g is dimensionally N times smaller than its prototype size at 1-g. Therefore, in an N = 15 (15-g) centrifuge experiment, the dimensions of the model pier are scaled by N (=15); density and stress at the prototype is equal to the model scale; force is scaled by $1/N^2$ ($=1/15^2$) and acceleration is scaled by N (=15). Basic scaling laws adopted for this experiment are those presented in Table 1.1, reproduced from Kutter (1992).

Table 1.1 Centrifuge scale factors for basic engineering parameters (after Kutter 1992).

Parameters	Symbols	Scale factors[1]
Acceleration, Gravity	a, g	N
Density	ρ	1
Length	L	1/N
Mass	M	$1/N^3$
Force	F	$1/N^2$
Stress, Strength	σ, s	1
Strain	ε	1
Time (Dynamic)	T	1/N
Frequency	F	N

[1] $N = \lambda_m/\lambda_p$, where λ = parameter of interest for prototype (*p*) and model (*m*), respectively.

CHAPTER 2: PRE-CENTRIFUGE TEST PREPARATION AT ONE-G

To perform grout installation in the 1/15th model scale in the centrifuge, practical issues, such as the small size of the model piers and the model grout, were evaluated by conducting experiments at the one-g level first. During this process, the instruments and tools to be used in the real experimental investigation in the centrifuge were developed, constructed and tested. In an effort to capture the resulting mechanisms of grout transfer into the soil at a small scale, a variety of grout types and pier installation methods were tested at one-g level in small buckets.

2.1 Primary Instruments and Grout Composition

2.1.1 Model Helical Pier

The dimensions of the prototype helical piers were selected based on technical documents provided by Precision Pier, USA (2005). The prototype pier consisted of a round tube shaft of 102 mm diameter, with one or two helices attached, which were of 406 mm diameter and 76 mm pitch. Due to the centrifuge scaling laws (Table 2.1) and considering 15-g applied to the model, the resulting model helical piers had a 6.4 mm outer diameter (O.D.), a 5.6 mm inner diameter (I.D.), a 444.5 mm long stem made of round brass tubing, and a helix of 23.6 mm diameter with a 5.1 mm pitch. A schematic is illustrated in Figure 2.1(a), and a prototype of a constructed model is shown in Figure 2.1(b). The model piers were constructed of brass tubing and the helices were soldered into place after being shaped with an appropriate pitch, using a custom designed helix jig (Figure2.2). The brass used for the models had a Young's Modulus of Elasticity E = 110 GPa, approximately half of steel's Young's modulus (200GPa), and a mass density ρ = 8400 kg/m^3, which was close to that of the steel (ρ = 7850 kg/m^3). Brass was selected due to its ease of workability, which made model construction quick and easily repeatable.

(a)

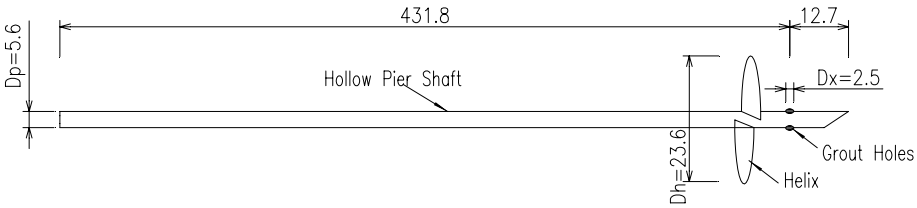

(b)

Figure 2.1 Model helical pier: (a) schematic (units in mm) and (b) photograph of constructed pier

Figure 2.2 Helix jig

2.1.2 Pressurized Grout Chamber

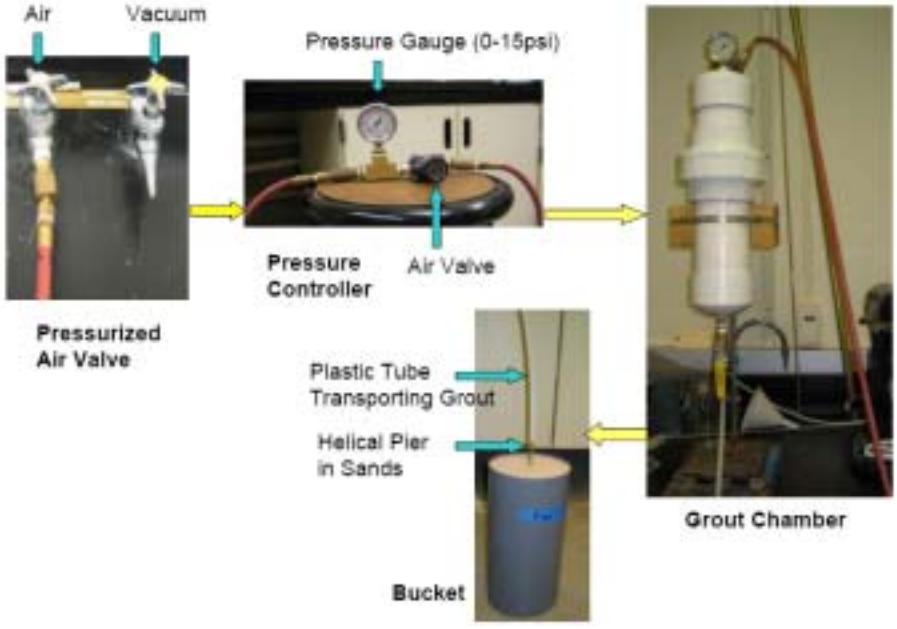

(a)

(b)

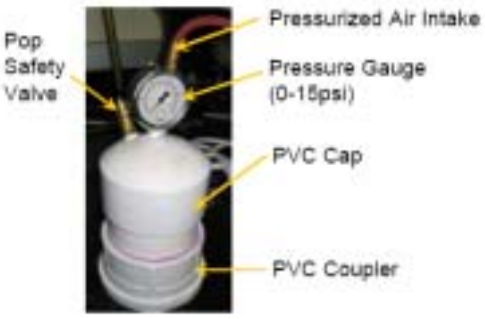

(c)

(a) grout pump system (b) grout chamber bottom (c) grout chamber top.
Figure 2.3 Test grout chamber

The designed grout delivery mechanism provided variable pressure control and could easily be filled with pre-mixed grout and cleaned for the one-g tests. It included a pressurized air valve, a pressure controller, a two-piece PVC tube grout chamber, and a pressure gage. PVC tubes were selected for their ease of mating (top and bottom pieces) and cleaning. A safety pressure gauge on the top of the grout chamber monitored the internal pressure and prevented it from exceeding the gage limit. Figure 2.3 shows the assembled PVC tube parts and coupler. The chamber was 102 mm in diameter, 254 mm high, with a total volume capacity of 2 Liters. It could support a maximum interior pressure of 0.103 MPa.

2.1.3 Soil Selection

In centrifuge testing, very fine sand was typically selected; however, for this application very fine grain sand would unduly limit the permeation of grout into the soil and clog the pier grout exit holes. Note that permeation grouting was controlled by the effective particle size at 10% passing, D_{10}, as obtained from a grain size distribution curve. To minimize clogging and assure permeation into the soil, sand of increasing effective grain size were tested starting with Nevada sand 120, 90, and 60, to Silica sand #30 (D_{10}: 0.09 mm, 0.13 mm, 0.13 mm, and 0.31 mm, respectively). Comparison between the grout installations in Nevada sand 60 and Silica sand #30 would be discussed in subsequent sections. For Nevada sand 120 and 90, severe clogging was encountered regularly at the soil/pier interface (the grout exit hole). The Silica sand #30 resulted in the most repeatable delivery and largest volume of placed grout and. As shown in Figure 2.4, this sand had a similar grain size distribution as that used by Nichols and Goodings (2000).

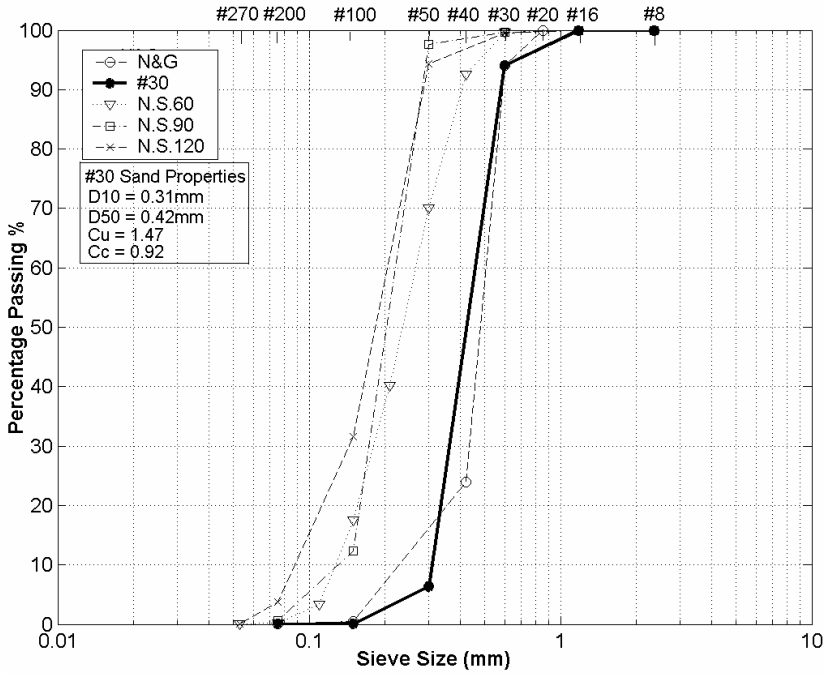

Figure 2.4 Grain size distribution curves for 1-g tests: Nevada sand (N.S.) 60, 90, 120, Silica sand #30 and Nichols and Goodings' sand (N&G)

2.1.4 Grout Mix Design

The grout was delivered through a shaft with an I.D of 5.6 mm, into the dry Silica sand #30 with its mean grain size (D_{50}) of 0.42 mm. To promote scale consistency between the grout and the surrounding soil, comparable with field applications, ultrafine cement was selected for the model grout. Ultrafine cement had a mean grain size smaller than 3 μm, 14 – 20% that of ordinary Portland cement (Nittetsu Cement Co., 2006). The ratio of the exit hole diameter (D_x) to the mean grain size (D_{50}) of the ultrafine cement (D_x/D_{50}) was 833. The larger this ratio was the less likely clogging at the exit hole would occur.

Different grout mixes were investigated for fluidity, permeability, and compressive strength. Four candidate grout mixes were considered as listed in Table 2.1. Additives were included to reduce the water content, improve fluidity, and to minimize bleeding and segregation. During centrifuge testing, it was expected that the mixed grout would most sit for approximately 20 minutes while the system was spinning to reach its target acceleration level. Since a goal of the research was to install grout in flight (while the centrifuge is spinning), the mix had to have a sufficiently long pot life to permit proper placement. Therefore, the fluidity of the grout mix over time was quantified using a flow cone test (ASTM C939). Five run-out times were recorded every 15 minutes over a one-hour duration (Figure 2.5). After one hour, Grout Mix C-1 had the shortest flow cone run-out time and minimum viscosity change: 18 secs at 15 min and 22 secs at 60 min. It was also found that Grout Mix B-1 at 60 minutes was too thick to flow through the flow cone.

Table 2.1 Grout mix summary (for 1-g tests)

Grout Mix Type	Cement	D_x/D_{50}[1]	Water Cement Ratio (w/c)	Pozzalite Clay[2]	Water Reducing Additive
A-1	TXI block cement[3]	170	0.80	5%	Adavaflow: 1%
B-1	TXI block cement[3]	170	0.70	2%	Adavaflow: 1%
C-1	NittetsuSuper Fine[4]	833	0.45	0%	Mighty-150: 1.5%
D-1	MC-500 cement[5]	600	0.45	0%	NS-200: 1.5%

Note: 1. D50 is for the #30 silica sand.
2. The percentages are by weight of cement.
3. Producer is TXI, Riverside, CA
4. Producer is Nittetsu Cement, Japan
5. Producer is Deneef Construction Chemicals, Houston, TX

The 3-, 7- and 14-day compressive strengths of Grout Mix C-1 were 15.1 MPa, 32.4 MPa and 33.8 MPa, respectively, highest among the 4 candidate grout mixes, as expected due to its low w/c ratio. For comparison, the 7-day compressive strengths of the four mixes are reported in Table 2.2. All candidate mixes had only minimal bleed and segregation after one-hour.

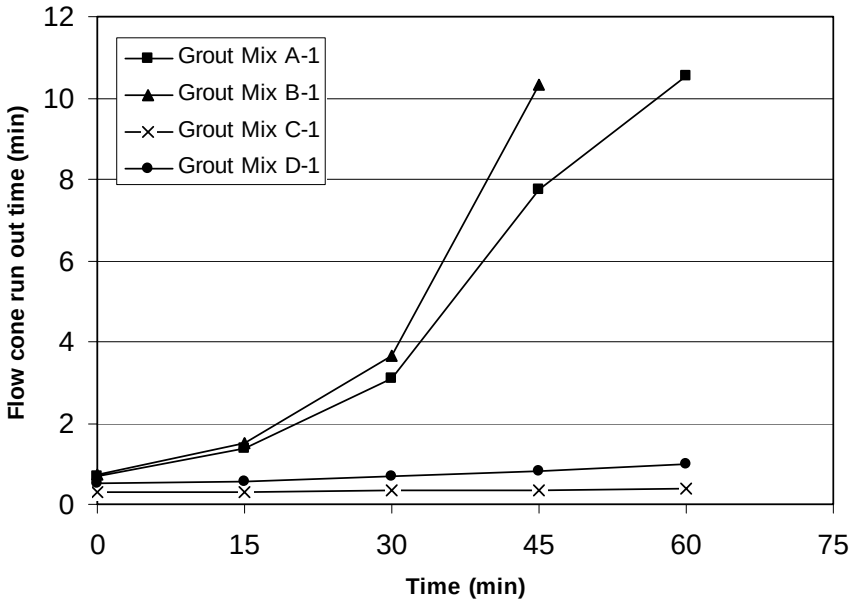

Figure 2.5 Flow cone run-out time vs. time based on Marsh cone experiments

Table 2.2 Seven-day compressive strength of grout in 1-g tests

Grout Mix Type	w/c ratio	Grout Strength (MPa)
A-1	0.80	14.5
B-1	0.70	15.3
C-1	0.45	32.4
D-1	0.60	20.9

2.2 One-G Bucket Tests

2.2.1 Experimental Setup

To investigate the grout and grout-pier system installation methods, a series of tests were conducted at one-g using the model piers and dry sand pluviated into buckets. These tests also served to evaluate the performance of the grout mix in the Nevada sand 60 and the Silica sand #30. Air pluviation was used to achieve a target above 80% relative density for both sands by suspending the hopper one meter above the sand surface in the bucket. Using a flexible hose with a sieve manually moved across the bucket surface area, air pluviation placement took approximately 50 minutes to deliver 0.1 m^3 of sand. Using this method, an average relative density of 82% was achieved.

Three different pier-grout installation schemes were considered as illustrated in Figure 2.6. In Scheme I, the grout installation used a model helical pier as same as shown in Figure 2.1. In Scheme II, the pier shaft was installed without the helix. The third

scheme differed from the second only in that an additional two sets of grout holes were drilled to increase the volume of deliverable grout.

In Scheme I, the model helical pier was first suspended vertically in the center of the bucket. Sand was then pluviated into the bucket surrounding the pier, until the pier end was embedded 203 mm into the sand. This mimicked the centrifuge installation process, where soil would first be placed at one-g around the model piers (the technology has yet to be developed to install the piers in flight). Subsequently the grout was installed at the same time as the pier was torqued. From this perspective, one might assume the effects of pier driving on soil confining stresses were minimal, compared with the soil modifications due to grout permeation. While torquing the pier at approximately 7–8 revolutions per minute (rpm), the grout was simultaneously delivered into the shaft from the grout chamber. During this torquing process, the helix drew the pier shaft approximately 51 mm further into the sand. For the pier shaft only cases (Scheme II and III), the shafts were embedded in the pluviated sand medium to a depth of 254 mm. Without any torque application, the grout was directly pressured into the shafts. In the above procedures, a constant grout chamber pressure of 83 kPa was maintained.

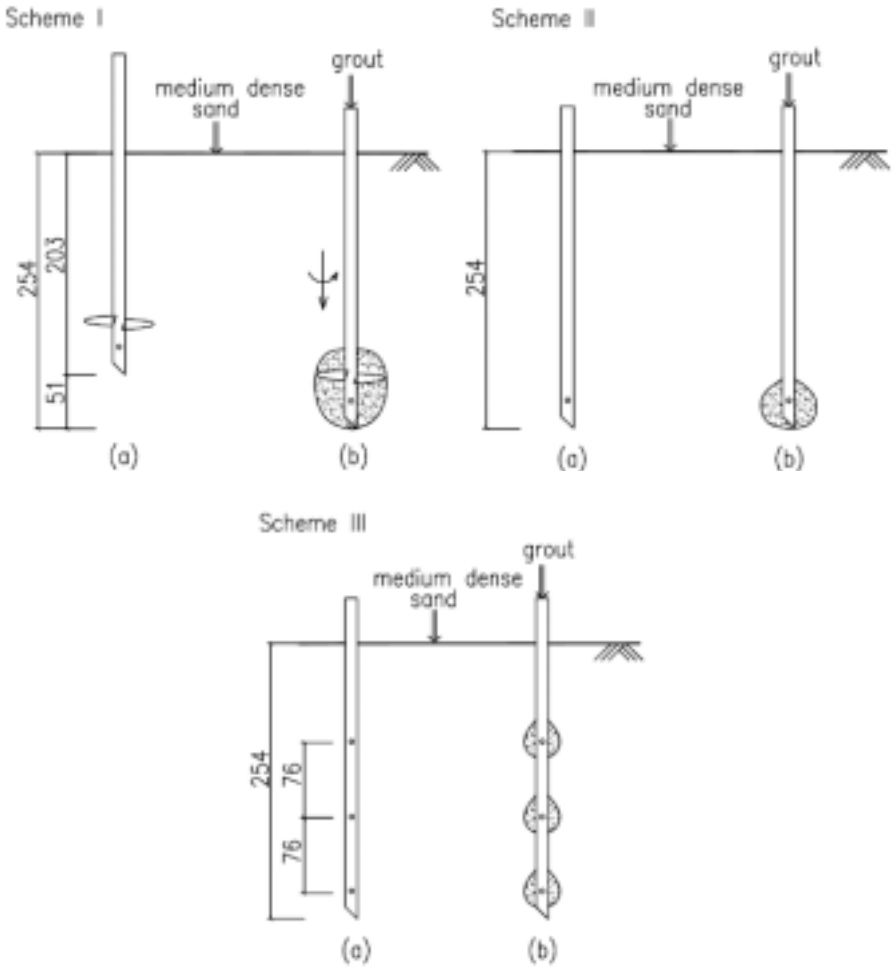

Figure 2.6 Schematic of the three installation schemes (all units in mm)

2.2.2 Results and Discussion

Each method was repeated at least seven times using Grout Mix C-1 in both the Nevada sand 60 and Silica sand #30 (Table 2.1). The buckets were excavated three days after grout installation, to facilitate physical inspection. Results are summarized as follows:

In Scheme I, the grout bulbs in the Nevada sand 60 were on average 25 mm in diameter ($4D_p$, where D_p is O.D. of the pier) and approximately 25 mm long; in Silica sand #30, grout bulbs were approximately 51 mm in diameter ($8D_p$) and 76 mm long (Figure 2.7 a and b).

For pier shafts with one set of holes used in Scheme II, grout bulbs in Nevada sand 60 were around 12.7 mm in diameter ($2D_p$) and 12.7 mm long. In Silica sand #30, grout bulbs were approximately 31.75 mm in diameter ($5D_p$) and 25 mm long (Figure 2.8 a and b).

For pier shaft with three-sets of holes in Scheme III, the grout bulbs were similar to those in Scheme II. It was observed that the lower two holes did not work well. The grout bulbs generated in the top holes from Scheme III were dimensionally similar to those in Scheme II. Each of these installation methods was highly repeatable, with similar grout sizes and geometries for individual runs of a given method.

a)  b) 

Figure 2.7 a) Grout bulb from Scheme I grout installation in Nevada sand 60 soil b) Grout bulb from Scheme I grout installation in Sand #30 soil (units in inches)

a) 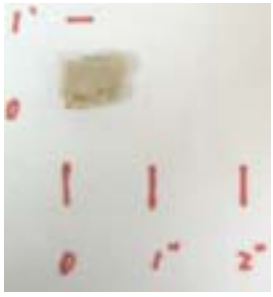 b) 

Figure 2.8 a) Grout bulb from Scheme II grout installation in Nevada sand 60 soil b) Grout bulb from Scheme II grout installation in Sand #30 soil (units in inches)

2.3 Summary and Impact on Centrifuge Test Design

Model helical piers, grout composition and installation of grouted, helical piers was investigated at one-g level, and the grout delivery through model piers was considered using different testing schemes in air pluviated dry sand. This work served as the preparation for subsequent centrifuge experiments. The findings might be summarized as follows: First, the presence of a helix during grout delivery resulted in approximately eight times more delivered grout volume. Secondly, the grout volume delivered in the Silica sand #30 was approximately 12 times that in Nevada sand 60. Thirdly, additional sets of grout holes aligned on the pier shaft proved not necessary. The largest grout bulbs obtained (approximately eight times that of the pier shaft diameter) were obtained when using the Silica sand #30 and pier with helix. These results provided insight into which pier-helix configurations, sand gradations and grout mixes were suitable for small-scale centrifuge experiments.

From the results of one-g level bucket tests, the following configurations were incorporated into15-g centrifuge tests:

- Only one set of grout holes was presented on the piers. No additional sets of grout holes were added.
- A single helix above the grout hole was chosen.
- Grout mix with ultra-fine cement was required, mix C-1 in the one-g test was selected as a baseline for the centrifuge test due to its adequate flowablility; low possibility of segregation, and high compressive strength.
- Atmospheric and 10psi pressure were selected as input pressure for the grout.

CHAPTER 3: CENTRIFUGE MODEL

3.1 Description of the Centrifuge

The National Geotechnical Centrifuge at UC Davis as shown in Figure 3.1 is the largest centrifuge in the United Sates (NEES@UCDAVIS, 2006). Its effective radius is 8.5 meters, and its available container area is 4.0 m^2. It is capable of carrying five-ton payloads to an acceleration of 75-g. Centrifuge support equipment include the in-flight actuators, in-flight CPT and various types of sensors. The centrifuge facility also includes a data acquisition system, which can record up to 160 channels of transducers.

The model container used for this project is a Flexible Shear Beam (FSB1) soil container (Figure 3.2), whose inside dimensions are of 1722 mm long, 686 mm wide, by 700 mm high. The FSB1 can hold up to 826.90-liter volume of sand. The 700mm height of the container provides a 10.5-m depth of soil at prototype for the 15-g model. The container depth will provide enough space for pier embedment, while minimizing the possibility of any influence of boundary effects.

Figure 3.1 The 9-m radius geotechnical centrifuge at UC Davis

Figure 3.2 Flexible Shear Beam (FSB1) soil container

3.2 Centrifuge Test Plan

Schematics of the centrifuge test plan are provided in Figure 3.3. The model includes 16 helical piers, one plain pier, the driving systems consisting of gear motors, racks and driving block, grout chambers, mac valves which electrically control the delivery of grout, the air pressure supplier, bender elements which tomographically image of the grouted pier geometry before and after grouting, the CPT devices and a hydraulic actuator. The model helical piers are brass shafts with an O.D. of 7.1 mm, an I.D. of 6.4 mm, a helix diameter of 25.4 mm, and a helix pitch of 5.1 mm (Figure 2.1). Parameters varied in the centrifuge test plan include: (i) grout type, (ii) grout installation pressure, (iii) pier embedment and (iv) pier torquing. These variables are listed in Table 3.1. It should also be noted that two plain piers were instrumented with strain gauges to measure the friction between the pier shaft and the sand.

The grout mixes used in the centrifuge tests are presented in Table 3.2. Nittetsu Super Fine cement grout was selected due to its good flowability, relatively long pot life and high strength. Grout with different w/c ratios and silica fume additives were used in the centrifuge testing program (Table 3.2). Note the range of w/c ratio is 0.4–0.6 by weight. A water reducing agent of between 1-1.5% was used and between 5-8% silica fume was used to evaluate the potential increase in cohesion of the matrix.

The centrifuge test is subsequently conducted in three phases:

I. Install the grout under different circumstances, perform the CPT test and load the two piers without grout installation at 15-g level.
II. After seven days of grout curing, load typical grouted helical piers as marked in Figure 3.3.
III. Excavate the FSB1 container, document the grout bulbs' dimensions and analyze the grout installation performance under different circumstances.

Table 3.1 Centrifuge test matrix

Pier Location	Helix	Motor rotation @ 5rpm	Embedment depth[1]		Grout Mix[2]				Air Pressure[3] (0.17 MPa)
			3.8m (256mm)	5.7m (381mm)	A	B	C	D	
A1, A2	√	√	√		√				
A3	√	√		√	√				
B1, B2	√	√	√			√			
B3, B4	√	√	√			√			√
B5, B6	√	√		√		√			
C1	√		√		√				
D1	√		√			√			
D2	√		√			√			√
E[4]			√						
F[4]	√		√						
G1	√	√	√				√		
G2	√	√	√				√		√
G3	√	√		√				√	

Note:
1. Prototype and model scale embedment depths are both listed, with model scale in parenthesis.
2. Grout mixes are summarized in Table 3.2.
3. Except for marked pier locations, grout is installed under atmospheric pressure.
4. Pier E & F are instrumented with strain gauges for loading test only, no grout installation is performed at these two locations.

Table 3.2 Grout mix summary (for centrifuge tests)

Grout Mix Type	Cement	Water Cement Ratio (w/c)	Silica Fume	Mighty-150 (water reducer)
A	Nittetsu Super Fine	0.45	0%	1.5%
B	Nittetsu Super Fine	0.60	0%	1%
C	Nittetsu Super Fine	0.40	5%	1.5%
D	Nittetsu Super Fine	0.40	8%	1.5%

Note: The percentages are by weight of cement

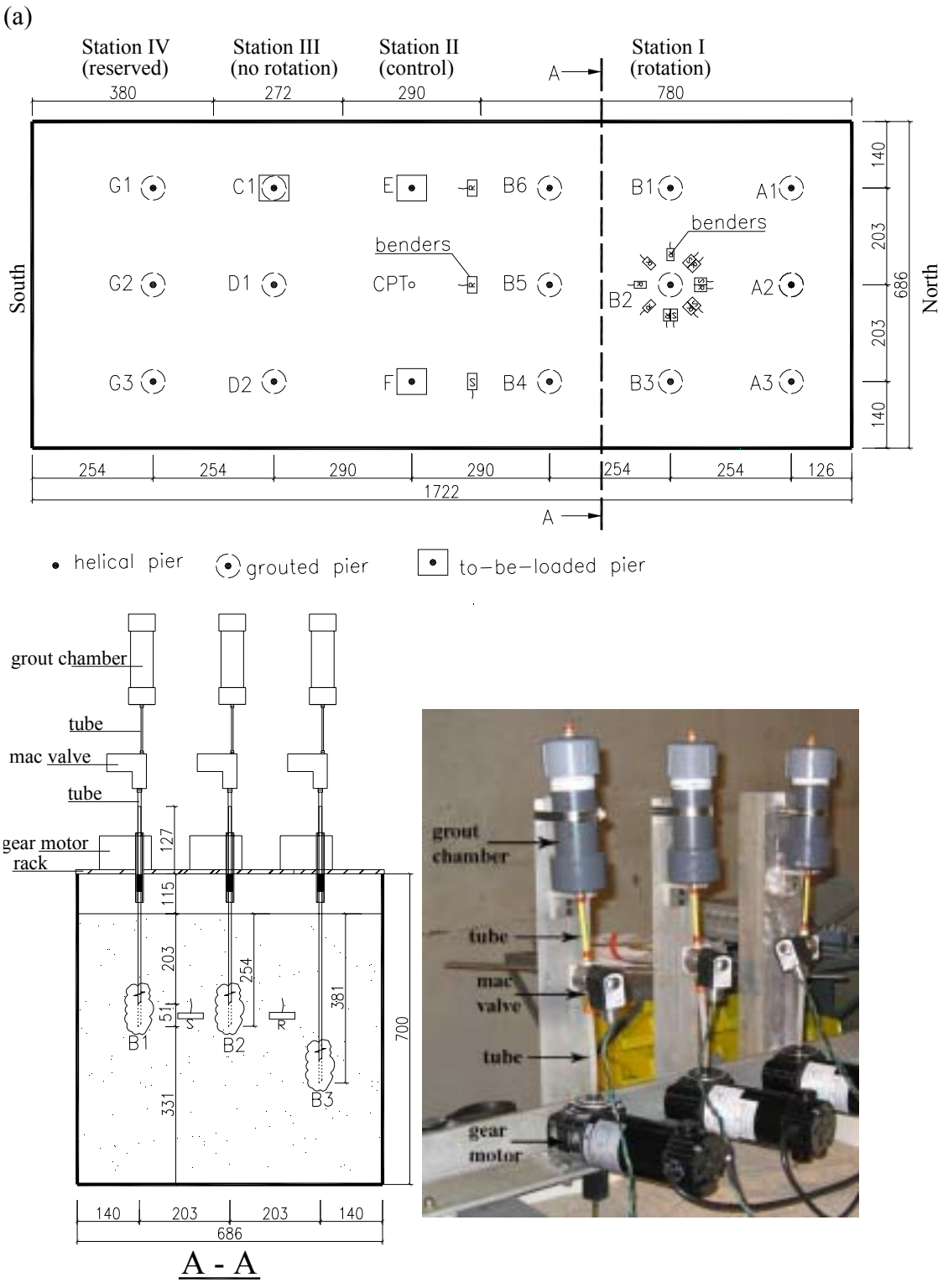

Figure 3.3 Centrifuge test layout in FSB1 (a) plan view (b) section view (c) photo of model elevation (units in mm, model scale)

3.3 Instrumentation

This centrifuge model was instrumented with strain gauges and bender elements. In addition, an in-flight CPT was performed and a hydraulic actuator equipped with load cell and displacement transducer used during testing. Paired strain gauges were bonded along two pier shafts to measure the friction between the sand and the shaft. Bender elements were embedded in the soil around pier B2 to image before and after grout installation. Besides these, three analog cameras were installed on top of the soil container to capture the images of pier driving, monitor the grout flow in the transparent tubes and track the pier deformation during the loading tests.

Before the centrifuge test, the calibration of instrumentations was conducted at one-g level, using the same terminals, amplifier channels, amplifier gain and jumper as would be used during the centrifuge test. The output recorded by a LabVIEW® data acquisition system was converted directly to parameter (displacement, axial load etc.) measurements without the use of instrument factors. Instruments were sampled at 4096 Hz. The instrument lists are presented in Tables 3.3 and 3.4.

Table 3.3 Instrument list for strain gauges, CPT devices and hydraulic actuator

Instr. No	Instr. Type	Engr. units	Location Description	Instr. Range	Calibr. factor [1] and units		Scale Factor
1	Strain gauge	-	Helical pier (lower)	-	289.1	N/v	1
2	Strain gauge	-	Helical pier (upper)	-	277.1	N/v	1
3	Strain gauge	-	Plain pier (lower)	-	318.9	N/v	1
4	Strain gauge	-	Plain pier (upper)	-	307.8	N/v	1
5	Actuator load cell	Lbs (N)	Actuator	500lbs	242.9	N/v	1
6	CPT	Lbs (N)	CPT device	500lbs	1.426	N/v	1
7	LVDT	mm	Actuator and CPT	10cm	15.2	mm/v	1

1. Calibration factor as applied to raw data.

3.3.1 Strain Gauges

One plain pier (non-helix) and one helical pier (pier E and F) with the same length of 254 mm were instrumented with a pair of 350Ω strain gauges (from Measurements Group, Inc.) at two elevations along the depth of the pier. The locations of the strain gauges are depicted in Figure 3.4.

The gauges were bonded onto the brass surface of piers. Two 30AWG wires (single conductor wires) were soldered to each gauge. The gauges were coated with a thin and flexible coating, 5-minute epoxy, to protect them from damage during the test and calibration.

The strain gauge circuit was arranged as a Wheatstone half-bridge circuit as shown in Figure 3.5. As shown in the figure, ε represents the active strain gauges, and another two same strain gauges as precision resistors are connected with the active gauges to complete the half bridge circuit. Because the two active gauges are electrically connected in opposite arms of the Wheatstone bridge, this configuration cancels the bending strains with equal magnitudes and opposite signs, therefore, minimizes the sensitivity to any bending. Figure 3.6 shows the physical connection of strain gauges, piers and wires. To convert the voltage readings to strain, and given that the excitation voltage is 5V DC, the following equation was used:

$$\frac{V_{out}}{V_{in}} = \frac{GF * \varepsilon}{2 + GF * \varepsilon} \qquad \textbf{(Equation 3.1)}$$

where, GF is the gauge factor fixed at 2.07 nom, specified by the gauge manufacturer.
The signals from the strain gauge bridge are amplified from the PVL amplifier for each pair of strain gauges. The gain of the amplifier was set at 500.

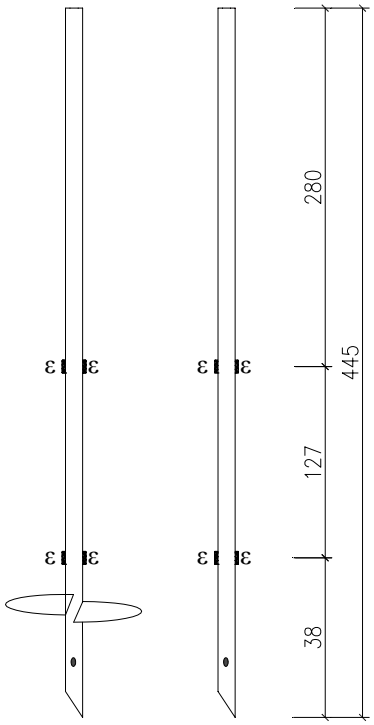

Figure 3.4 Strain gauge locations on one helical pier and one non-helix pier (side view) (units in mm)

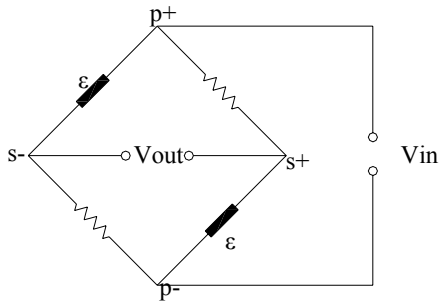

Figure 3.5 The Wheatstone half-bridge configuration for strain gauges

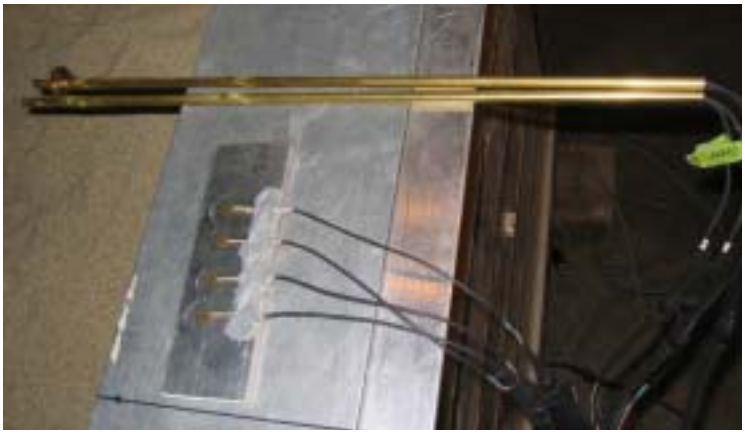

Figure 3.6 Photo of strain gauges' Wheatstone half bridge connection

3.3.2 Bender Elements

The primary objective of using the bender elements is to perform tomographic imaging of the grouted pier geometry before and after grouting. These images could be used to compare with physical inspection and also to calculate shear wave velocity of the grout-sand matrix. From these results, a future test matrix might be adjusted before completing the grout installation. The components of the bender element test system are shown in Figure 3.7.

There are two types of benders: source benders and receiver benders. The source benders are provided with a voltage excitation from the bender driver and the source benders bend and cause a shear wave. The receiver benders are bent by the shear wave and they generate an excitation record. Thus, shear wave velocity data can be collected along multiple ray paths through the soil, grout and pier as depicted in Figure 3.8.

In the centrifuge model, one polar array of benders was placed around a pier where grout bulb was anticipated (pier B2). The array was placed at a model diameter of 152 mm to assure the benders would not be buried in the grout (the maximum diameter of the grout bulb was estimated to be less than 90 mm). Then two rows of free field benders were placed in the soil to evaluate the soil conditions and confirm the hardware functions

as well. One row was placed at 254 mm depth and one at 381 mm depth, the two depths to be treated with grout (Figure 3.9). The channel list of bender elements is provided in Table 3.4.

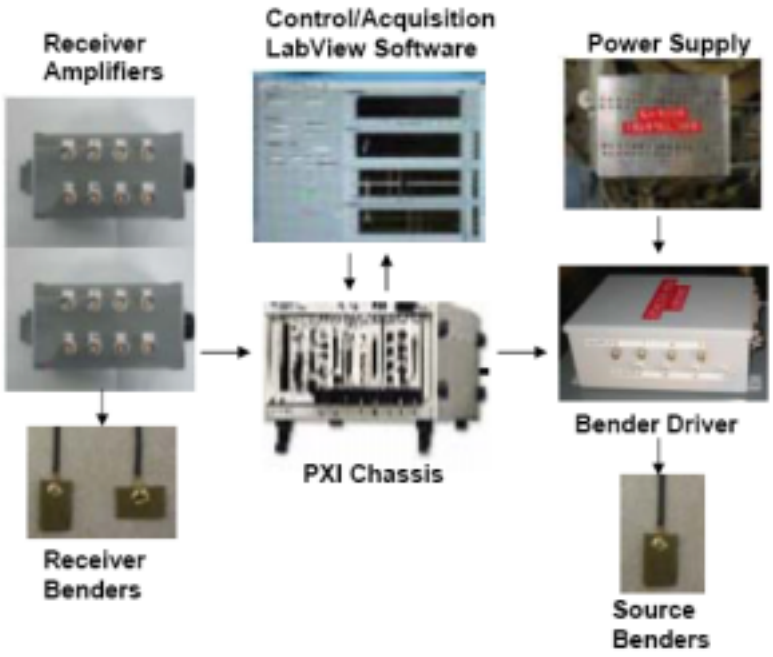

Figure 3.7 Component schematic of bender elements (Brandenberg et al., 2006)

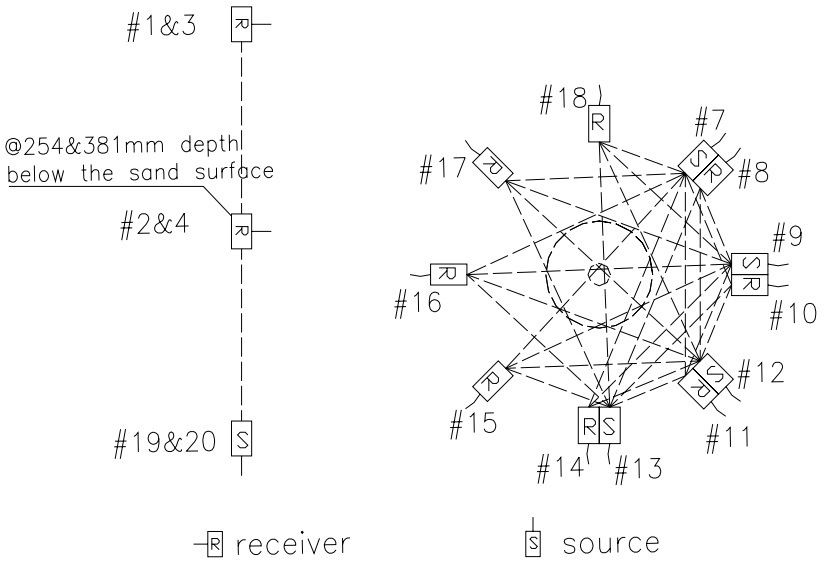

Figure 3.8 Bender element ray path traces and locations

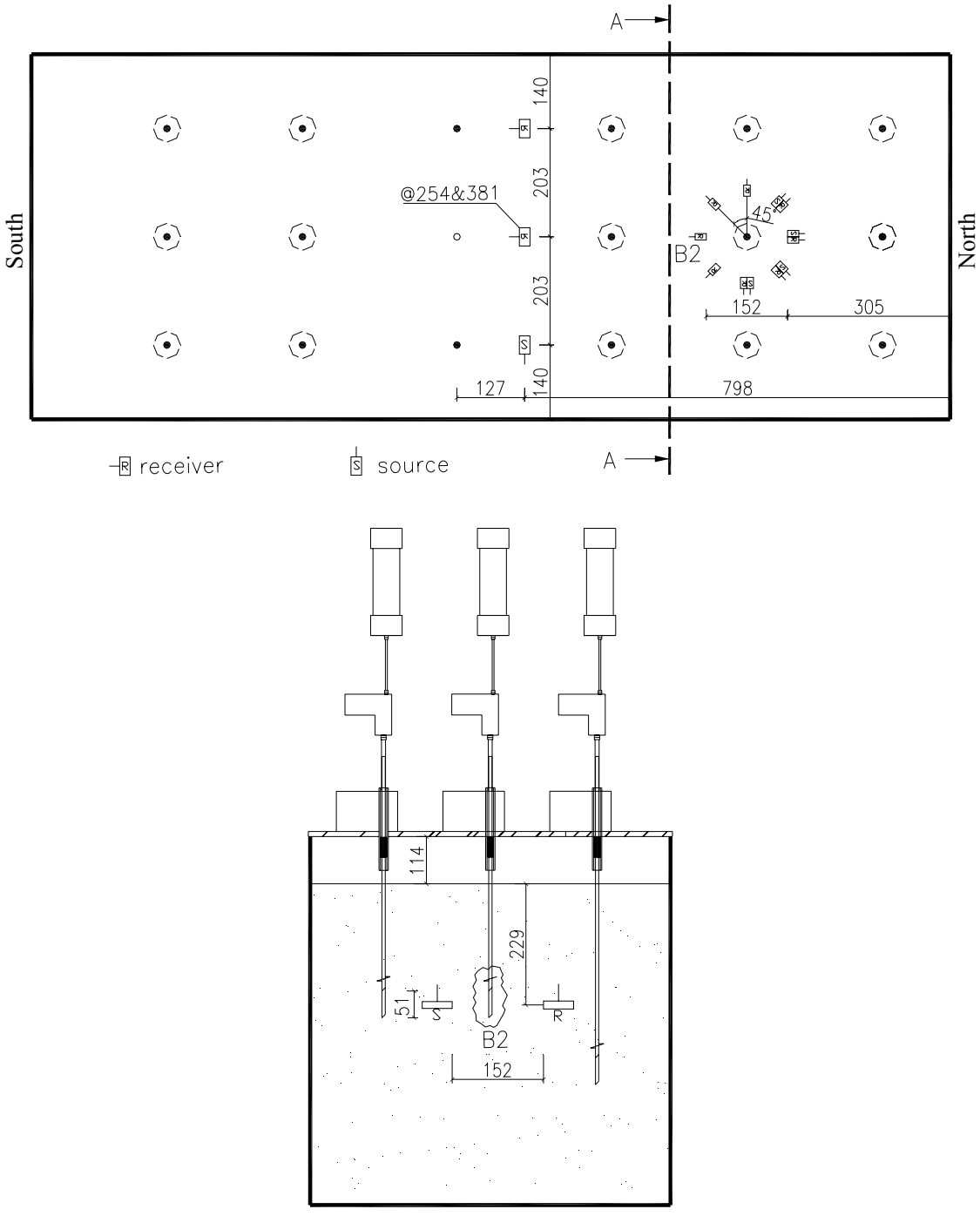

Figure 3.9 Bender element layout in FSB1 (plan and section view) (units in mm, model scale)

Table 3.4 Channel list for bender elements

No.	Source	Channel (bender driver)	Receiver	Channel (receiver amplifiers)
1	# 7	ch1	# 1	ch1
2	# 9	ch2	# 2	ch2
3	# 12	ch3	# 3	ch3
4	# 13	ch4	# 4	ch4
5	# 19	ch5	# 8	ch5
6	# 20	ch6	# 10	ch6
7			# 11	ch7
8			# 14	ch8
9			# 15	ch9
10			# 16	ch10
11			# 17	ch11

3.3.3 Cone Penetration Test Apparatus and Hydraulic Actuator

The cone penetration test (CPT) apparatus developed by UCD NEES consists of a cone penetrometer (Figure 3.10) and a linear variable differential transformer (LVDT). The embedded strain gauges inside the tip of the cone penetrometer allow a real time continuous measurement when the tip is being pushed into the ground at a constant speed. The strain gauges provide the compressive load on the tip, which can be converted into tip pressure. The cone penetrometer has a base diameter of 6 mm with an apex angle of 60 degree, resulting in a projected area of 28.26 mm^2. Simultaneously, the linear motion of the cone penetrometer is recorded by an LVDT. The signals from the strain gauges at the cone tip are amplified with one PVL amplifier. In this test, the gain of the amplifier was set at 1000.

Boundary conditions can have a significant influence on the CPT measurements. With respect to the side boundary condition, Renzi et. al (1994) reported that, "for dense sand, the soil container diameter must be 50 times the diameter of the cone to eliminate the effect of side boundary on CPT tip resistance". For the CPT device used in this experiment, the cone is located in the center of the soil container, with a distance of 340 mm (57 times the cone diameter) from the container side. Phillips and Valsangkar (1987) investigated the influence of bottom boundary conditions on CPT data and indicated that, for a 10 mm cone, the bottom boundary effects are seen starting at a vertical distance of 10 to 12 cone diameter. For this test, the minimum distance between the cone tip and the container bottom is 478 mm, about 80 times of cone diameter.

By replacing the cylindrical probe in the CPT device with an Interface 500 lbf load cell, a hydraulic actuator is established as shown in Figure 3.11 (a). Axially load the pier, a pin point connection consisting of a steel ball and a square block was constructed and attached on top of each pier planned for loading [Figure 3.11 (b)].

Figure 3.10 Cone Penetrometer (photograph courtesy to NEES site)

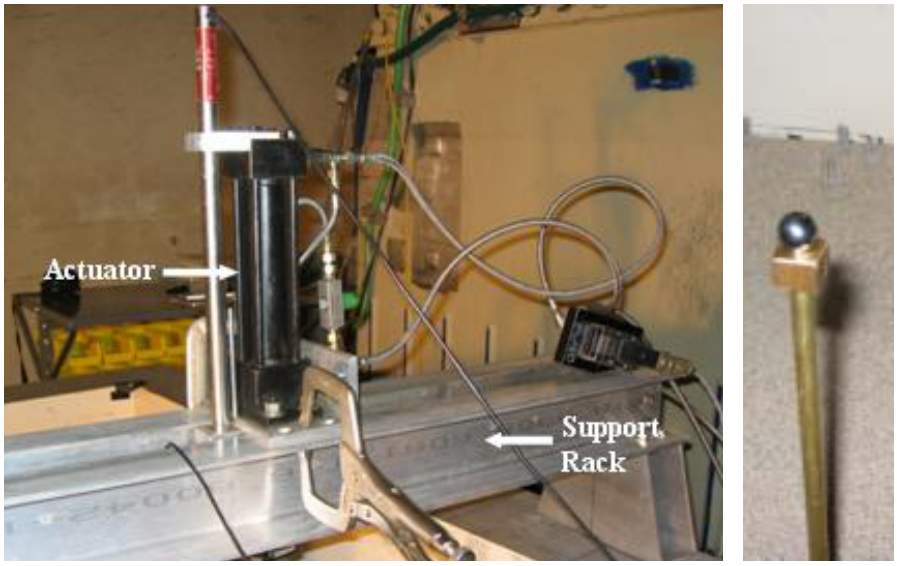

(a) (b)

Figure 3.11 Loading test set-up: (a) hydraulic actuator (b) loading pin point

3.4 Soil Profile and Pluviation

The soil used for the centrifuge testing was #30 sand obtained commercially from White Cap Construction Supply. Figure 3.12 shows the grain size distribution curve for this soil. For comparison, the #30 sand obtained for the 1-g tests is also shown. These two sands have fairly similar grain size distributions. A majority of the sand particles are retained on the 50 sieve, with a small percent of fine aggregates present. According to the USCS, this type of sand is considered poorly graded.

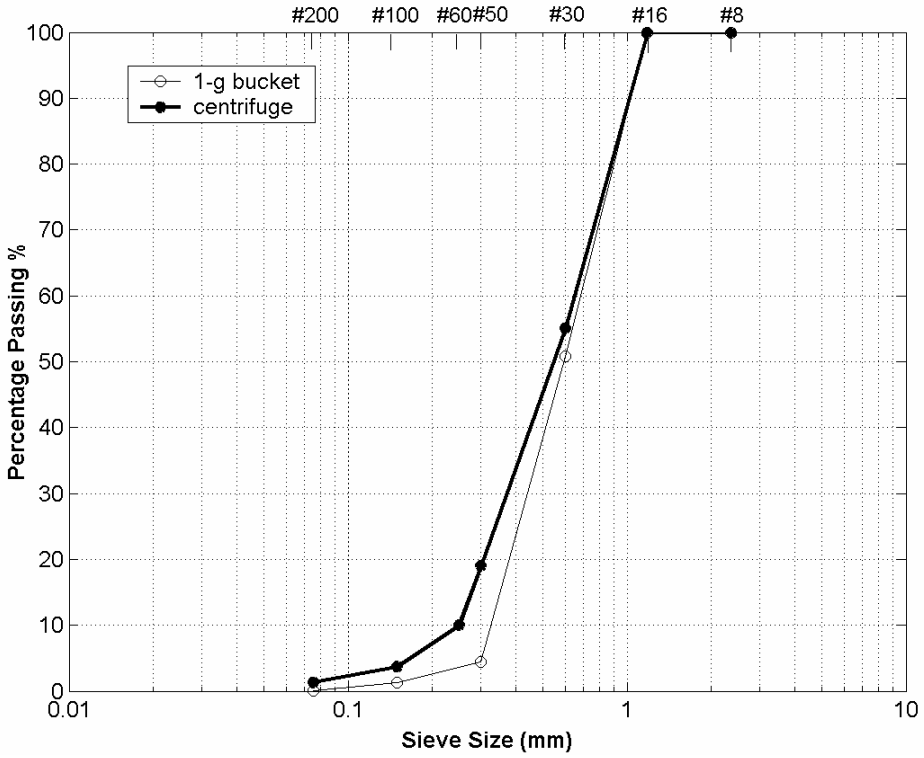

Figure 3.12 Grain size distribution curve for #30 silica sand used in 1-g bucket tests and in centrifuge tests

By performing ASTM maximum and minimum density tests (ASTM D 42530-00 and ASTM D 42540-00, respectively), the obtained minimum density is 13.9 kN/m^3, and the maximum density is 16.6 kN/m^3. Other mechanical properties of the #30 sand are summarized in Table 3.5. An in-place a relative density of 80% was selected as the target density for the centrifuge model.

Table 3.5 Properties of the #30 sand used in the centrifuge test

D_{10}	D_{50}	Cc	Cu	ω (moisture content)	γ_{max} (max unit weight)	γ_{min} (min unit weight)
0.28	0.55	2.32	0.79	0.16%	16.6 kN/m^3	13.9 kN/m^3

The sand was placed into the FSB1 soil container by air pluviation, also known as sand raining, to obtain a uniform relative density soil. The relative density was determined by dropping the sand at different speeds and heights. Although the moisture content is also a factor that influences the repeatability of the relative density, the sand was pluviated directly as dry sand due to its low moisture content of 0.16%.

To obtain the target relative density, a steel chamber with known volume and weight was used to calibrate the pluviator (Figure 3.13). In each calibration trial test, the unit weight (γ) of sand in the chamber was calculated first, then Equation 3.2 was used to calculate the relative density (D_r).

$$D_r = \frac{\gamma - \gamma_{\min}}{\gamma_{\max} - \gamma_{\min}} * \frac{\gamma_{\max}}{\gamma} * 100\% \qquad \textbf{(Equation 3.2)}$$

After several trial tests, a relative density of 83.8% was achieved steadily with the soil unit weight of 16.1kN/m^3. During these trial tests, the bottom screen of the pluviator was placed 82 cm above the sand surface, and the driving motor speed was set at 70rev/min. In the following discussion, the pluviation process is described.

First, the sand was poured into the top opening and then the pluviator was moved in a smooth motion back and forth across the container to let the sand fall evenly into the container. At the same time, the pluviator was pulled upward gradually with the screen elevation kept at a constant elevation. During the pluviation, if the sand landing on the edges of the container rolled into the container, a looser structure may form. Therefore, four angel irons were placed along the edges to prevent the sand falling from edges. In addition, even a light wind may disturb the results. Therefore, doors were shut tightly during the entire procedure. To achieve a consistent soil profile and maintain a relatively smooth and level sand surface, the pluviation was stopped every couple of inches of elevation to level the surface with a vacuum. Figure 3.14 partially depicts this procedure.

Figure 3.13 Pluviator calibration

Figure 3.14 Sand pluviation

3.5 The Centrifuge Model Construction

The centrifuge model was prepared and constructed in the following five steps:

- Placement of the bottom set of free-field benders:
  The #30 sand was pluviated in the container to an elevation of 203 mm, and then vacuumed to a level and smooth surface. The bottom set of free-field benders was then laid in the middle of the container.

- Placement of the four long piers in the container:
  Pluviation was continued to an elevation of 280 mm, burying the benders, then the sand surface was leveled with a vacuum, and the four long piers were carefully seated long piers on top of the sand layer with string supports. The strings were stretched and pasted onto the container edges to locate and fix the piers (Figure 3.15)

- Placement of the bender circle and the top set of free-field benders:
  Pluviation was continued for another 76 mm. Subsequently, a 152 mm diameter clamp hose and a straight string were used to precisely locate the bender polar array and free-field benders (Figure 3.16).

- Placement all short piers in the container:
  Pluviation continued for another 51 mm. The sand was leveled and strings were pasted and fastened onto the edges of the container to locate the short piers. All remaining 12 short piers were placed at string intersections (Figure 3.17).

- Final filling of the container:
  The remaining 114 mm of sand was pluviated to the top the container, the support strings were remove down then the sand surface was carefully vacuumed and leveled, especially around the piers. The completed view of the completely constructed centrifuge model is presented in Figure 3.18.

After moving the centrifuge model onto the arm, all the instrumentations and racks were mounted onto the container edges with clamps; all the cables were bundled and fixed onto the container too. The instrumented centrifuge model is depicted in Figure 3.19.

Figure 3.15 Pier layout in FSB1 at step two

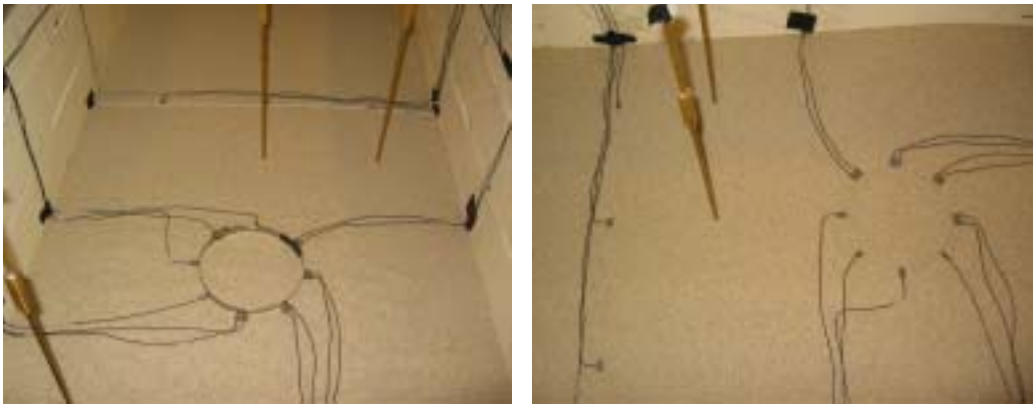

Figure 3.16 Bender layout (L: benders in placement and R: after completion)

Figure 3.17 Pier layout in FSB1 at step four

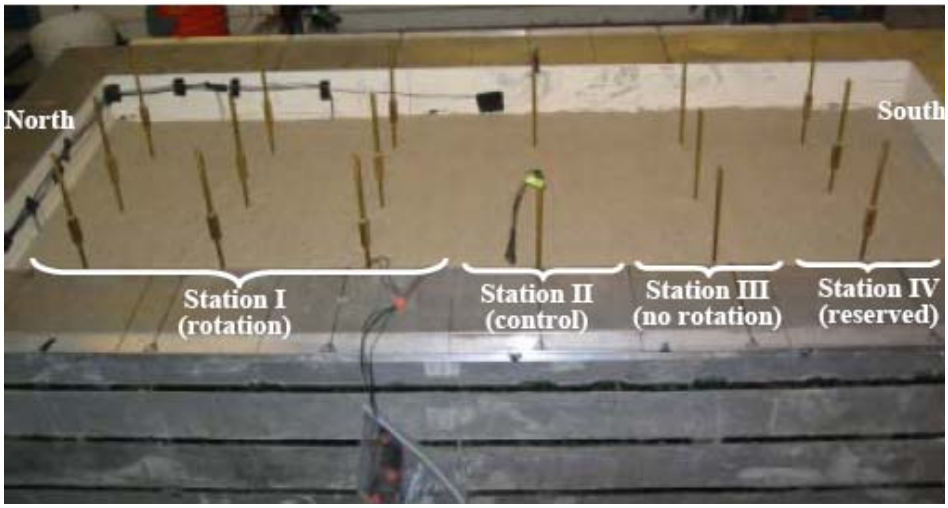

Figure 3.18 Constructed Centrifuge Model

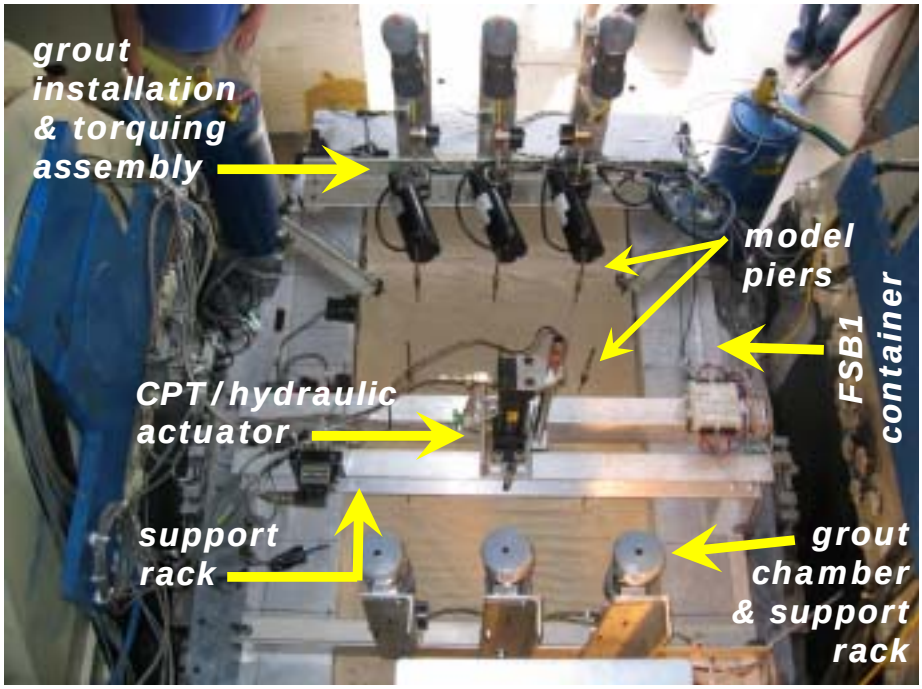

Figure 3.19 Model on centrifuge arm

CHAPTER 4: CENTRIFUGE TEST SERIES: EXECUTION AND RESULTS

In this chapter, the execution of the centrifuge test is described, and observations made during testing are noted. Results after physical inspection are presented and discussion of findings provided.

4.1 Centrifuge Test Series

The centrifuge test began on June 9th, 2006 and finished on June 16th, 2006; seven spins were conducted in total. The complete test series and observations during the spin are reported in the time sequence presented in Tables 4.1 - 4.6. Due to the lack of previous work on centrifuge testing of grouted helical piers, the model was carefully monitored during and after each spin. Modifications were made to improve the grout installation and pier driving during each spin. In total, seven spin cycles were conducted (Tables 4.1-4.6). In general, during each spin, a number of piers were grouted and torqued simultaneously. Other testing procedures were also performed, such as CPT profiling and axial loading of select piers. Activities performed during each spin-up-down cycle are noted by the dashed boxes surrounding the plan schematic below each of Tables 4.1-4.6 and described in the following:

- **First Spin**

  The first spin cycle was performed on June 9th, 2006.

  Four minutes before spinning, 35 ml of Grout A (w/c: 0.45) was placed into each chamber (A1, A2 and A3) at 11:07am. Mixing of the grout was continued until just prior to placement to minimize the chance of hardening at one-g.

  The model was spun up at 11:11am and reached 15-g four minutes later. After the model reached 15-g, the grout control valves and motors for piers A1, A2 and A3 were enabled simultaneously. The motor rotation speed was 5 rpm for three piers. The piers rotated and moved downward far slower than the target 25 mm/min (helix pitch is around 5 mm, therefore, 5 mm/round * 5 rpm = 25 mm/min). It was observed that the long pier's (A3) moving rate (5 mm/min) was twice as fast as the short piers (A1&A2). Subsequently, CPT profiling was conducted. However, the CPT feedback jumper was broken during the spin, therefore no data was recorded at this point in time. At the end of the spin, the benders were tested and the data at non-grout locations was collected successfully. At 11:38am, the model was spun down. The first spin lasted for 7 minutes in total.

After spinning down, the grout chambers were opened. It was observed that more than 70% by weight of dry grout remained in the grout chamber.

- **Second Spin**

The second spin was executed on June 9th in the afternoon.

During the interval between the first and second spins, a 13 x 25 x 51 (mm) extra weight of 120 g was cast and mounted onto each pier (B1, B2 and B3) to increase the driving load. About 7 minutes before this spin, 35 ml of grout B (w/c: 0.6) was placed into each chamber (B1, B2 and B3) separately.

The model was spun up at 2:47pm and reached 15-g at 2:51pm. Pier B1, B2 and B3 started to rotate at the same time at 5 rpm, and the grout control valve was simultaneously hooked up. Though the driving load was increased with the extra weight, no obvious increase in the draw down rate was observed. Subsequently, CPT profiling was attempted. Unfortunately, the hydraulic fluid spilled out during the spin, and the CPT failed.

At 3:15pm, the model was spun down. The grout remaining in the chamber was dried and weighted to estimate the residual. It was estimated that approximately 70% by weight of dry cement remained in the chamber, tube and pier for B1, 70% for B2, and 90% for B3.

- **Third Spin**

On June 12th in the afternoon, the third spin was performed.

Before the third spin began, all four piers were preloaded and rotated by hand at 1-g one full revolution to engage the helix. Subsequently, 35 ml of grout B was placed in each of chambers B4, B5, B6 and D2 five minutes before spinning. To mechanically shorten the grout flow time, thus hopefully reduce the grout segregation, a funnel was attached to the bottom of each chamber and a larger diameter tube (I.D.: 9.5 mm) was used to substitute the 6.4 mm I.D. tube.

At 4:11pm, the model was spun up and reached 15-g at 4:14pm. Subsequently, the grout control valves and the rotation motors for pier B4, B5 and B6 were simultaneously turned on. The rotation speed of the three motors was held at 5 rpm. In this spin, the piers were found to rotate and draw downwards much faster than the former two spins, at approximately 19 mm per minute, close to the target 25 mm per minute. At the end of the spin, CPT profiling was conducted and the CPT data was successfully recorded.

After 21 minute of spinning at 15-g, the model was spun down at 4:32pm. Though the funnel was added and a larger diameter tube was substituted, little obvious improvement of grout injection was noticed. It was estimated that approximately 30 - 40% of grout was injected into soil.

- **Fourth and Fifth Spin**

The major objectives for fourth and fifth spins were to collect the loading data at 15-g for the ungrouted plain pier E and ungrouted helical pier F. The capacities of ungrouted piers measured in these two spins would be useful for comparison with those of grouted piers.

The two spins were conducted on June 13th in the afternoon. Spin four started at 12:13pm, reached 15-g at 12:17pm and stopped at 12:35pm. This spin lasted for 18 minutes in total. Spin 5th started at 15:27pm, reached 15-g at 15:30pm and spun down at 15:49pm, for 19 minutes total

- **Sixth Spin**

The sixth spin was conducted on June 15th, 2006.

Before the spin started, pier G1, G2 and G3 were preloaded and rotated by hand, at 1-g. In an effort to alleviate grout segregation at 15-g, silica fume was added to the grout mix. Seventy ml of grout C (w/c: 0.4 and silica fume: 5% by weight of cement) was placed into chamber G1 and G2 (35 ml each), with 35 ml of grout D (w/c: 0.4 and silica fume: 8% by weight of cement) added to chamber D. All grout was placed into the individual pier chambers 14 minutes before spinning.

At 2:29 pm, the model was spun up and reached 15-g at 2:43 pm. Subsequently, the grout control valves and the motors for all three piers were simultaneously turned on. The rotation speed of the three motors was held at 5 rpm. The piers were observed to rotate and move downward around 20 mm per minute. The model was spun down at 3:02pm.

During post-test inspection, it was observed that no grout was left in chamber G1 and G3, and about 20% by weight of dry grout remained in chamber G2.

- **Seventh Spin**

To measure the capacity of a grouted helical pier, the seventh spin was performed on June 16th, 2006.

Pier C1 was believed to have a successful grout bulb, therefore an attempt at loading was pursued. However, this pier wasn't prepared for loading and unfortunately, the pier buckled under axial compression prior to soil bearing failure. This spin started at 2:05pm, reached 15-g four minutes later, and spun down at 2:42pm.

As described above, modifications applied during the spin cycles were on grout installation and pier driving. The next two sections will focus on these two topics.

4.1 In-flight Grout Installation

To minimize the potential for grout hardening prior to completion of the installation, the mixing of grout and the delivery of grout into the chamber was always the final step before spinning up the centrifuge. In the first two spins (Tables 4.1-4.2), grout segregation was observed to be much more severe and faster than that observed during the one-g tests. The Nittetsu Super Fine cement grout worked well at one-g without obvious segregation observed after more than two hours. One potential explanation may be as described below.

If the grout is placed at one-g level, the cohesion between the particles can restrain the particles from separating; hence, the segregation appears mainly due to Brownian motion, which takes a long time to appear. However, at 15-g centrifugal acceleration, the cohesion cannot overcome the cohesion force, therefore, segregation occurs rapidly and the heavier cement particles are forced outward.

To alleviate segregation, in the third spin (Table 4.3), several approaches were attempted during the experiments. As a first attempt, a funnel was attached to the bottom of each chamber (Figure 4.1) and a larger diameter tube (I.D.: 9.5 mm) was used to substitute the 6.4 mm I.D. tube to mechanically shorten the grout flow time, while helping guide the grout downward towards the pier and hopefully reducing the grout segregation. However, there was no obvious improvement observed with this solution compared with the former spin results.

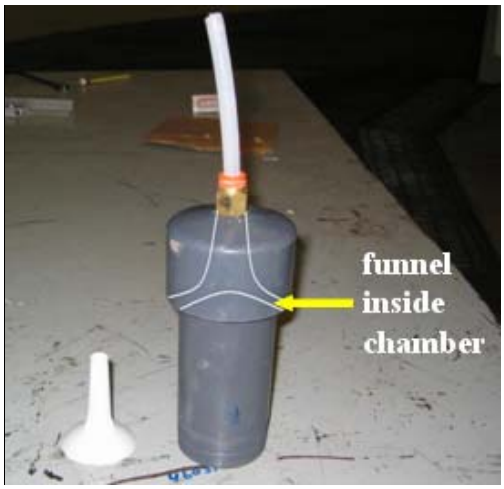

Figure 4.1 Funnel and grout chamber

During spin six, an additive was sought to increase the cohesion between the cement particles and water molecules, such that 15-*g* inertial force due to the centrifuge could be overcomed by the grout mix, thus minimizing segregation. Silica fume, which is described by ACI 116R (2006) as “very fine non-crystalline silica produced in electric arc furnaces”, was selected as the additive. By adding fine silica fume, millions of very small particles were now included in the cement water mixture. The very fine aggregates

of silica fume (medium particle size: 0.5μm) fill in the spaces between cement grains (medium particle size: 3μm), hence reducing the water content and increasing the cohesion between particles. The newly adjusted grout mixes with silica fume added and a lower water cement ratio was tested in the 6th spin. Test results and discussion are presented in Section 4.5.

4.2 Pier Driving

With the 5 mm helix pitch and the gear motors speed set at 5 rpm, the piers are theoretically drawn down at a rate of 25 mm per minute. However, lower pier driving rates were encountered during the first centrifuge spin. This was due to the light weight of the pier and its installation assembly. This problem was resolved as described below.

In the first spin, the obtained moving rates were less than 20% of the theoretical rates (only 5 mm per minute for the long piers and 2.5 mm per minute for the short piers). The long piers moved twice as fast as the short piers due to their additional self-weight (Table 4.1). To resolve this problem, before the second spin, an extra mass (120g) was clamped onto the pier shaft to increase the driving load (Figure 4.2). However, there was no noticeable increase in the draw down rate. It may be that the voids in the sand around the helix during the pluviation caused the problem observed in the second spin. Therefore, before the third spin up, all four piers were preloaded and rotated by hand, at 1-g one full revolution to engage the helix. During the third spin, the piers were found to rotate and move downwards much faster than the former two spins, at approximately 19 mm per minute, close to the target 25 mm per minute. This technique was adopted in subsequent testing.

Figure 4.2 Extra weights added to increase the moving rate

Table 4.1 First spin of the centrifuge test (units in prototype scale, unless otherwise noted)

1st Spin **Date**: June 9th, 2006 **Time**: 11:11am *spun up* 11:15am *reached 15-g* 11:38am *spun down*					
Pier No. [1]	**Grout Type [2]**	**Air Pressure[3] (MPa)**	**Depth [3] (m)**	**Motor Speed (rpm)**	**Description and Observations**
A1	grout A	0.101	3.81	5	1. The grout was placed into the chamber at 11:07am. 2. The grout segregated much more severely at 15g than at 1g, more than 70% by weight of dry grout remained in the grout chamber. 3. The piers rotated and moved downward far slower than target 25 mm/min. The long pier's (A3) moving rate (5 mm/min) was twice as fast as the short piers (A1&A2). 4. The benders were tested and the data at non-grout locations was collected.
A2	grout A	0.101	3.81	5	
A3	grout A	0.101	5.72	5	
C1	grout A	0.101	3.81	N/A	
CPT	-	-	-	-	CPT feedback jumper broke during the spin, the CPT test failed.

Note: 1. The piers tested in each spin are circled in the picture below each table;
2. Table 4.2 gives the grout mix summary.
3. 0.101 MPa equals to atmospheric pressure.

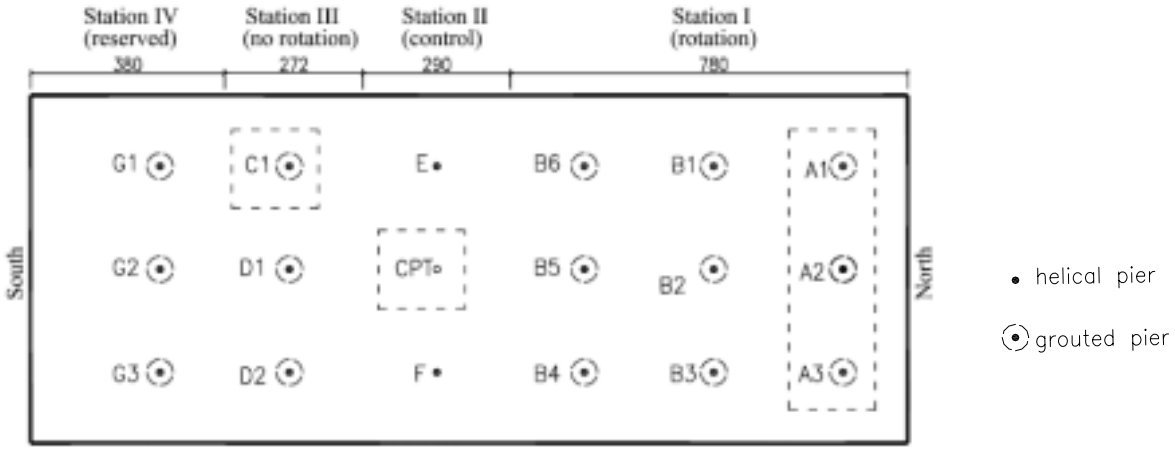

First Spin Case (dashed boxes indicate areas of testing) (all units in mm, model scale)

Table 4.2 Second spin of the centrifuge test (units in prototype scale, unless otherwise noted)

2nd Spin **Date:** June 9th, 2006 **Time:** 2:47pm *spun up* 2:51pm *reached 15-g* 3:15pm *spun down*					
Pier No.[1]	**Grout Type [2]**	**Air Pressure [3] (MPa)**	**Depth (m)**	**Motor Speed (rpm)**	**Description and Observations (model scale)**
B1	grout B	0.101	3.8	5	1. The grout was placed into the chamber at 2:40pm. 2. A 13 x 25 x 51 (mm) extra weight of 120 g was mounted onto each pier to increase the driving load, however, no obvious increase in the draw down rate was observed. 3. The grout remaining in the chamber was dried and weighted to estimate the residue. It is estimated there was approximately 70% by weight of dry cement left in the chamber, tube and pier for B1, 70% for B2, and 90% for B3.
B2	grout B	0.101	3.8	5	
B3	grout B	0.171	3.8	5	
D1	grout B	0.171	3.8	N/A	
CPT	-	-	-	-	Hydraulic fluid spilled out during the spin, and the CPT failed for the second time.

Note: 1. The piers tested in each spin are circled in the picture below each table;
2. Table 4.2 gives the grout mix summary.
3. 0.101 MPa equals to atmospheric pressure.

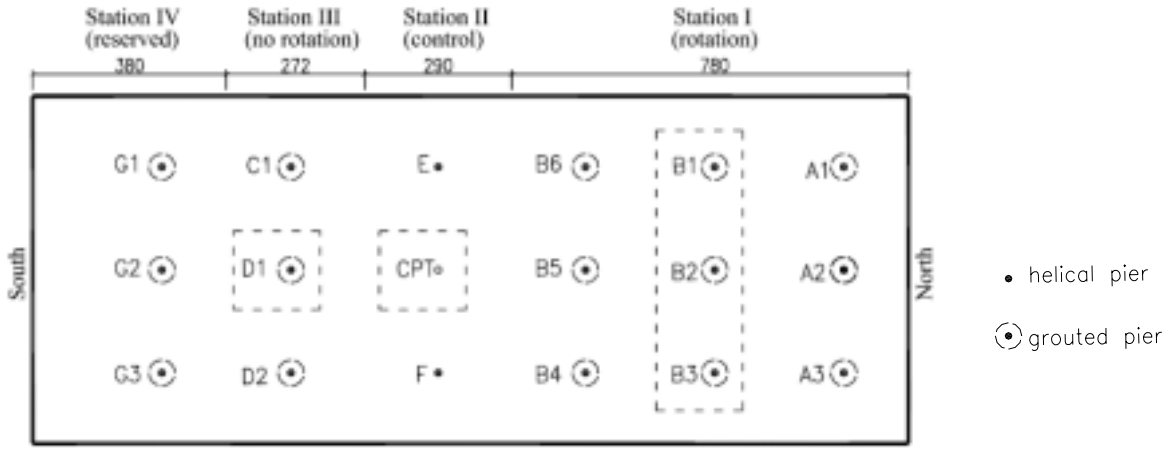

Second Spin Case (dashed boxes indicate areas of testing) (all units in mm, model scale)

Table 4.3 Third spin of the centrifuge test (units in prototype scale, unless otherwise noted)

3rd Spin **Date:** June 12th, 2006 **Time**: 4:11pm *spun up* 4:14pm *reached 15-g* 4:32pm *spun down*					
Pier No.[1]	**Grout Type [2]**	**Air Pressure [3] (MPa)**	**Depth (m)**	**Motor Speed (rpm)**	**Description and Observations (model scale)**
B4	grout B	0.171	3.8	5	1. The grout was placed into the chamber at 4:06pm. 2. Before spin, the pier was preloaded and turned one full revolution, after spinning to 15-g, the piers were observed to rotate at correct speed (5rpm) and moved downward much faster, 19 mm/min, much closer to the theoretical 25 mm/min. 3. A funnel was attached to the bottom of each chamber, however, little obvious improvement was noticed, 30 - 40% of cement in grout was injected into soil. 4. The data for benders with grout installation were collected.
B5	grout B	0.101	5.7	5	
B6	grout B	0.101	5.7	5	
D2	grout B	0.101	3.8	N/A	
CPT	-	-	-	-	CPT test succeeded.

Note: 1. The piers tested in each spin are circled in the picture below each table;
2. Table 4.2 gives the grout mix summary.
3. 0.101 MPa equals to atmospheric pressure.

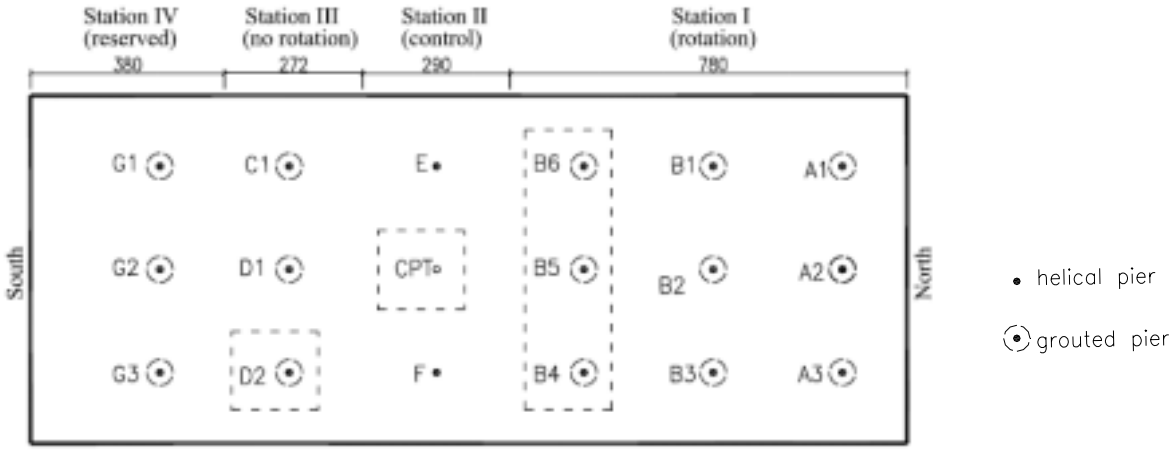

Third Spin Case (dashed boxes indicate areas of testing) (all units in mm, model scale)

Table 4.4 Fourth and fifth spin of the centrifuge test (units in prototype scale, unless otherwise noted)

4th Spin & 5th Spin Date: June 13th, 2006 Time: 12:13pm *spun up* 12:17pm *reached 15-g* 12:35pm *spun down* 15:27pm *spun up* 15: 30pm *reached 15-g* 15:49pm *spun down*			
Pier No.	**Depth (m)**	**Pier**	**Description and Observations (model scale)**
E	3.8	helical pier (w/ helix)	The loading block fell off under pressure during the loading.
F	3.8	plain pier (no helix)	Loading was completed successfully.

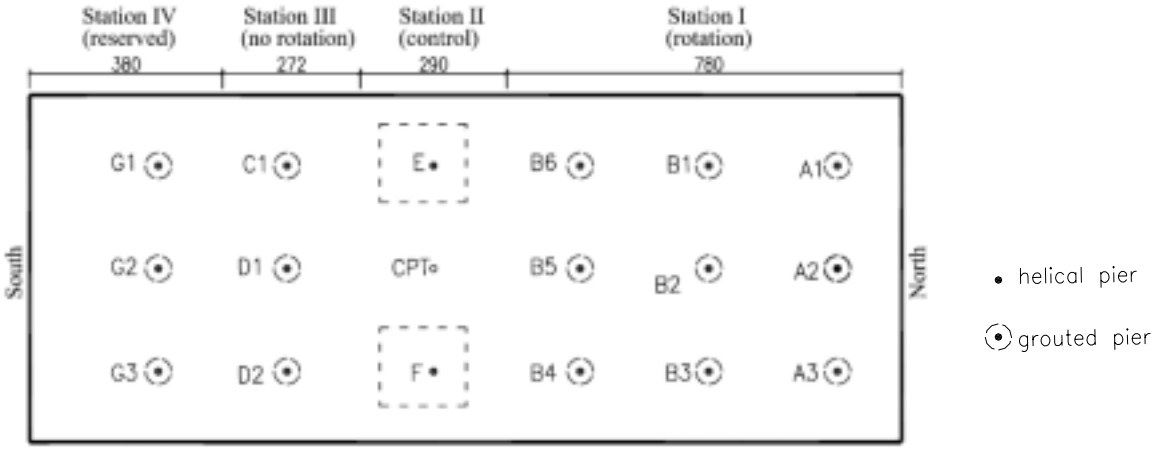

Fourth and Fifth Spin Case (dashed boxes indicate areas of testing) (all units in mm, model scale)

Table 4.5 Sixth spin of the centrifuge test (units in prototype scale, unless otherwise noted)

6th Spin **Date**: June 15th, 2006 **Time**: 2:39pm *spun up* 2:43pm *reached 15g* 3:02pm *spun down*					
Pier No.[1]	**Grout Type** [2]	**Air Pressure** [3] **(MPa)**	**Depth (m)**	**Motor Speed (rpm)**	**Description and Observations (model scale)**
G1	grout C	0.101	3.8	5	1. The grout was placed in the chamber at 2:25pm. 2. No grout left in grout chamber G1 & G3, about 20% by weight of dry grout left in chamber G2.
G2	grout C	0.171	5.7	5	
G3	grout D	0.101	5.7	5	

Note: 1. The piers tested in each spin are circled in the picture below each table;
2. Table 4.2 gives the grout mix summary.
3. 0.101 MPa equals to atmospheric pressure.

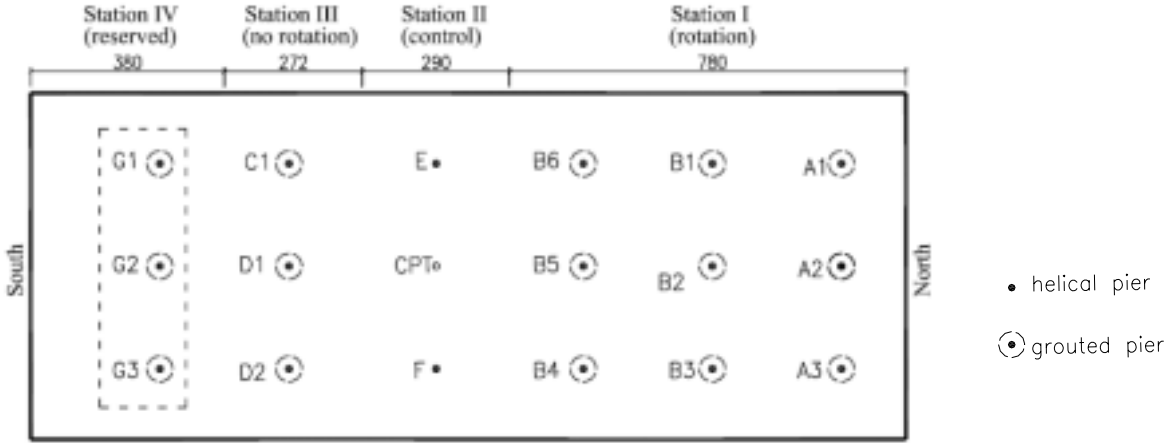

Sixth Spin Case (dashed boxes indicate areas of testing) (all units in mm, model scale)

Table 4.6 Seventh spin of centrifuge test (units in prototype scale, unless otherwise noted)

7th Spin **Date**: June 16th, 2006 **Time**: 2:05pm *spun up* 2:09pm *reached 15g* 2:42pm *spun down*					
Pier No.[1]	**Grout Type** [2]	**Air Pressure** [3] **(MPa)**	**Depth (m)**	**Motor Speed (rpm)**	**Description and Observations (model scale)**
C1	grout A	0.101	3.8	N/A	This pier was not prepared for axial loading, however, it was believed to have a successful grout bulb and an attempt at loading pursued. Unfortunately, the pier buckled under axial compression prior to soil bearing failure.

Note: 1. The piers tested in each spin are circled in the picture below each table;
2. Table 4.2 gives the grout mix summary.
3. 0.101 MPa equals to atmospheric pressure.

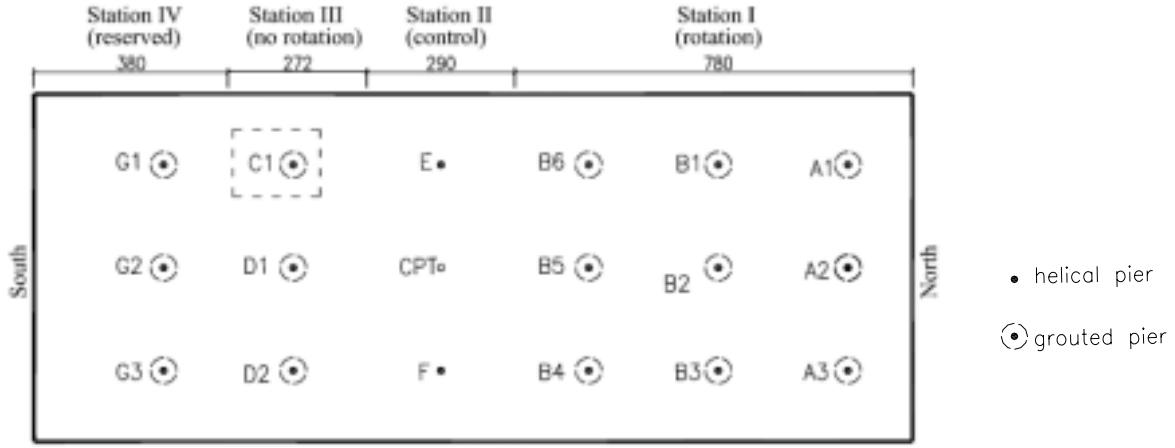

Seventh Spin Case (dashed boxes indicate areas of testing) (all units in mm, model scale)

4.2 CPT Results

4.2.1 CPT profile

CPT profiling was conducted in the middle of the FSB container shown in Figure 3.2. The CPT probe is capable of penetrating into the sand to a depth of prototype depth of 1.6 m. It should be noted that this is much shallower than the model pier embedment (Figure 4.3). The CPT extended less than half of the depth of the short pier and one third of the depth of the long pier.

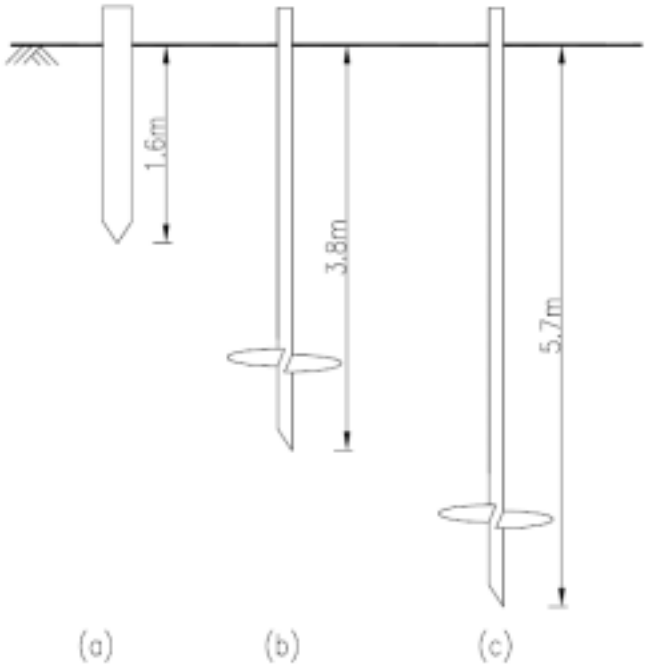

Figure 4.3 Embedment depth of: (a) penetration cone (b) short helical pier (c) long helical pier (prototype units)

The original CPT data is filtered in the frequent domain, using a Butterworth filter with a cut-off frequency of 5 Hz. This filtering process is summarized in a Matlab program, which is reported in Appendix A. The filtered CPT data is presented in Figure 4.4.

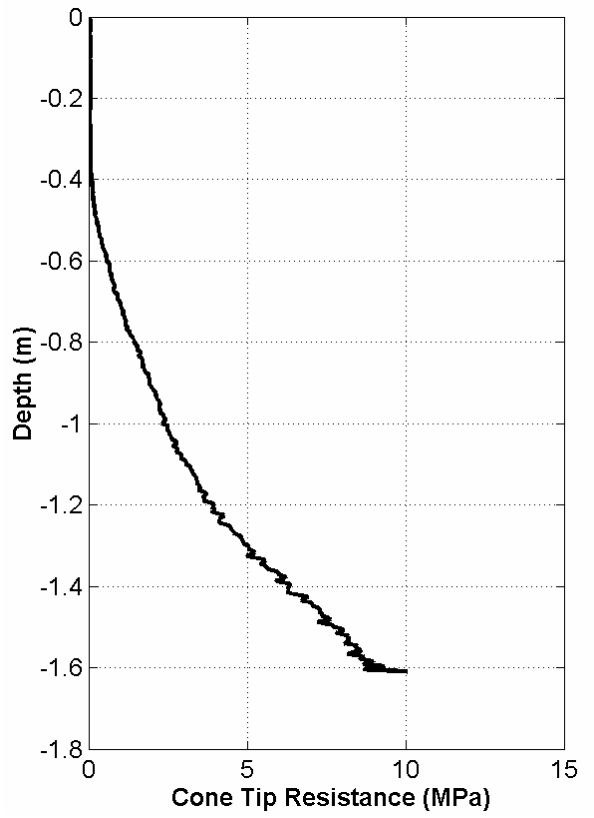

Figure 4.4 CPT profile (prototype units)

4.2.2 Correlation of CPT Data with Mechanical Properties of Soil

To characterize the in-place mechanical properties of the sand in the model, published empirical correlations are used. Cone tip resistance may be correlated with relative density using a general correlation equation by Kulhawy and Mayne (1991):

$$D_r^{\,2} = \left(\frac{1}{Q_F}\right)\left[\frac{(q_c / p_a)}{(\sigma_o' / p_a)^{0.5}}\right] \qquad \textbf{(Equation 4.1)}$$

where, p_a = atmospheric pressure (about 100 kPa);
σ'_o = vertical effective stress;
q_c = cone tip resistance;
Q_F = an empirical constant of the least-square regression.

As suggested in Kulhawy and Mayne (1991), Q_F is selected as 305 for sands with medium compressibility. To use Equation 4.1, and in light of the shallow penetration of the CPT, the deepest region of measured cone resistance is used. From Equation 4.1, the

relative density (Dr) at 1.6 m is calculated to be 80.4%, which is fairly close to the Dr from the pluviation calibration, 83.8%.

Similarly, one may be interested in the in-place strength of the sand. Robertson and Campanella (1983) investigated the relation between cone tip resistance and friction angle, suggesting:

$$\phi' = \tan^{-1}[0.1 + 0.38 * \log(q_c / \sigma'_0)] \quad \textbf{(Equation 4.2)}$$

where, ϕ' = soil friction angle

σ'_o = vertical effective stress;

q_c = cone tip resistance;

Based on Equation 4.2, the calculated friction angle ranged from 42˚ to 46˚ between the depths of 1.4 m and 1.6m. Considering the estimated relative density of 80.4%, and a friction angle rang of between 42˚ and 46˚, the in-place sand for the model may be characterized as dense sand (Meyerhof, 1956).

4.3 Compressive Strength Tests on Grout for Each Spin

After placing the premixed grout (40 mL) into each chamber before spinning, the remaining mixed grout was cast into 50 mm diameter cylinders and its compressive strength was tested on the same day of the spin, and between 18-24 days post-placement. Table 4.7 presents a summary of the grout compressive strength for each pier location.

Table 4.7 Compressive strength of grout using in centrifuge tests

Pier Location	Spin No.	Grout Type	w/c ratio	Grout Strength (MPa)	
A1, A2, A3	1st	Grout A	0.45	24-day	34.2
B1, B2, B3	2nd	Grout B	0.60	24-day	23.7
B4, B5, B6	3rd	Grout B	0.60	21-day	23.9
C1	1st	Grout A	0.45	24-day	34.2
D1	2nd	Grout B	0.60	24-day	23.7
D2	3rd	Grout B	0.60	21-day	23.9
G1, G2	6th	Grout C	0.40	18-day	38.8
G3	6th	Grout D	0.40	18-day	40.7

The range of compressive strengths is 23.7-40.7 MPa, with a mean of 30.4 MPa, and standard deviation of 7.4 MPa. It is noted that these strengths are slightly high for typical grout, yet more comparable to conventional concrete mixes. This high strength may be attributed to the ultra-fine cement with excellent performance on strength and low w/c ratio which is slightly lower than most field placed grout. However, as noted previously,

these mixes performed well at one-g using the pier-sand combinations used during centrifuge testing.

4.4 Bender Element Test Results

Tomographic images were constructed before and after grouting while the centrifuge spun at 15-g using a polar array of bender elements placed around pier B2, as shown in Figure 4.5a. Bender elements were energized after spin-up to 15-g, and before and after grouting at this location. Figure 4.6 shows the recorded signals from the receiver. Travel times were picked from the recorded signals, the region between the bender elements was discretized into pixels, and the unknown values of shear wave velocity of the pixels was obtained by tomographic inversion. The resulting tomograms are presented in Figure 4.7. The tomograms showed that the shear wave velocity of the soil was uniformly about 210 m/s before grouting, which is fairly reasonable for dense sand. Furthermore, the 38-mm diameter grout bulb (Figure 4.5a) near the center of the array after grouting was clearly identifiable. The predicted shear wave velocity of the grout (600 m/s) is lower than the expected values (approximately 1570-1800 m/s), and additional studies are needed to identify the cause of this error. Note also that the pixel sizes are large compared with the size of the grout bulb, hence the shape and position of the bulb could not be accurately resolved. A parametric-based approach is being studied to improve upon these limitations.

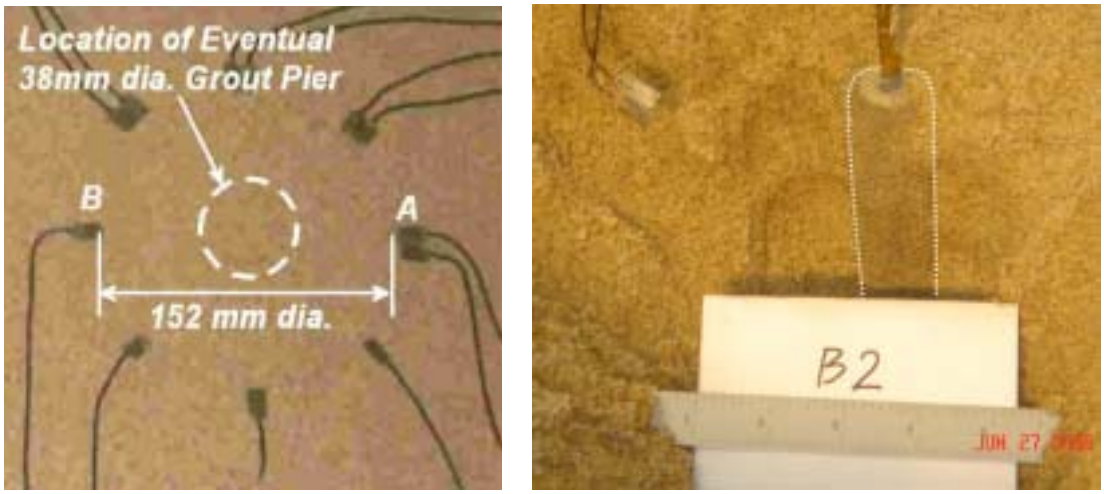

(a) **(b)**

Figure 4.5 (a) Photograph of polar array of bender elements during model construction prior to testing on centrifuge showing location where bulb was eventually grouted (courtesy to S. Brandenberg), (b) Photograph of evaluation of grouted bulb at pier location B2 (with polar array of bender elements instrumented) during the excavation (units in model scale)

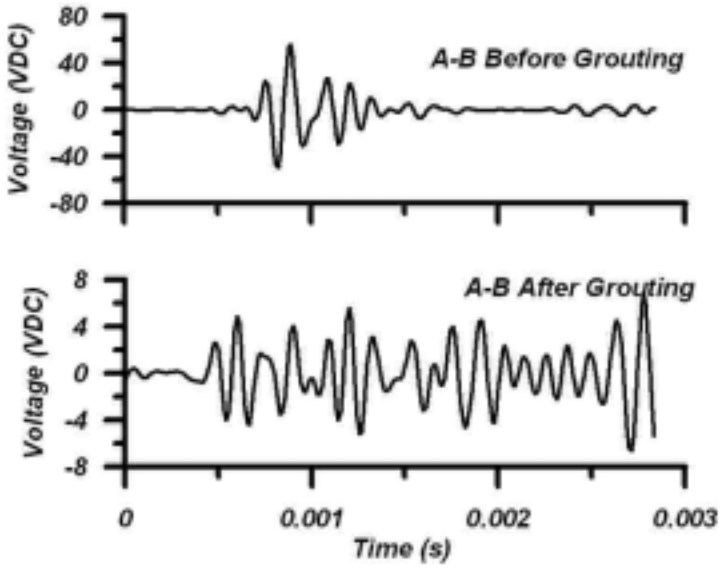

Figure 4.6 Shear wave signals from wave source bender (A) to receiver bender (B) before and after grouting (courtesy to S. Brandenberg)

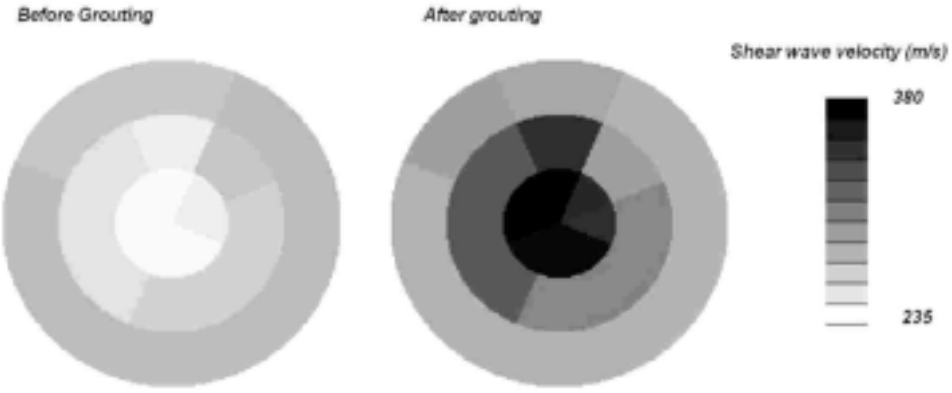

Figure 4.7 Tomography depicting shear wave velocity profiles before and after grouting (courtesy to S. Brandenberg)

4.5 Observations and Results of Grout Installation

Ten days following the final spin, after grout was thoroughly hardened, the model container was physically excavated and each grouted helical pier carefully removed from the container. Results of the 15 excavated grout installed piers are summarized in Table 4.8, where the geometric notations used are depicted in Figure 4.8; dimensions listed in Table 4.8 are prototype dimensions, which are obtained by multiplying the model dimensions by the centrifuge scale N = 15. Photographs of all excavated piers and grout bulbs are shown in Figure 4.9. Appendix B provides additional photographs of the observed installed grout.

It is noted that of the 15 piers grouted, 40% (six) suffered from poor performance of the installation procedure. For example, four helix-pier connections failed during torquing, while two piers suffered from grout leakage during installation, due to a poor seal at the funnel-chamber connection. Despite these failures, much information can be obtained from the successfully grouted piers, as well as those that were unsuccessful, for future testing.

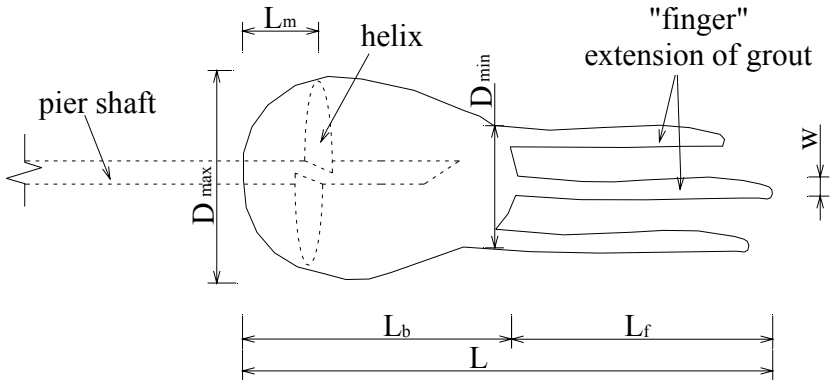

Figure 4.8 Notation used for dimensional analysis of grout bulbs


B1


B2


B4


B5


C1

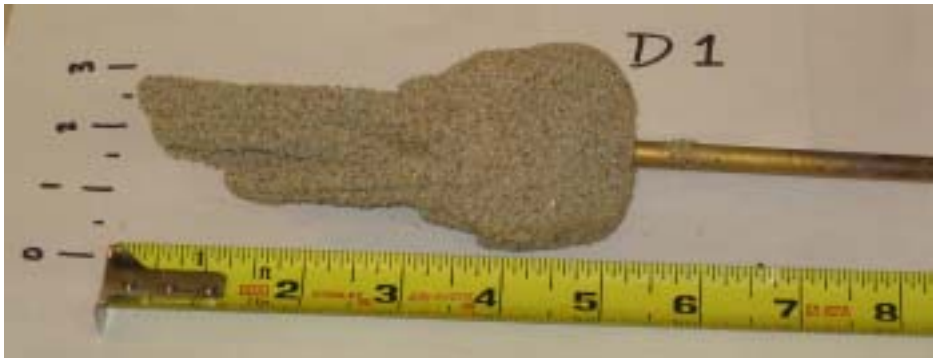
D1


D2

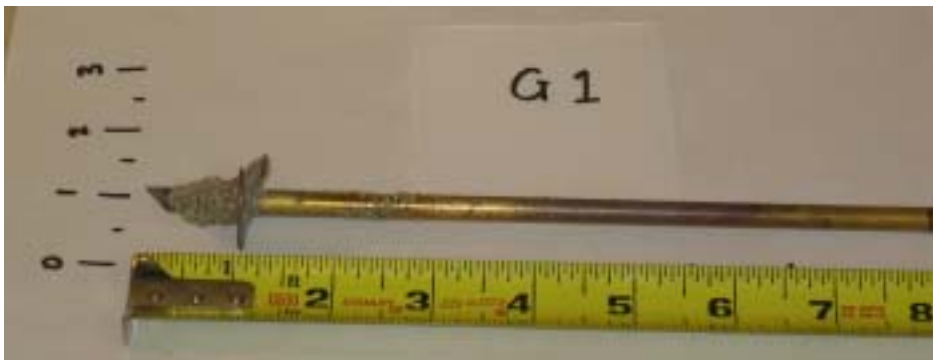
G1


G3

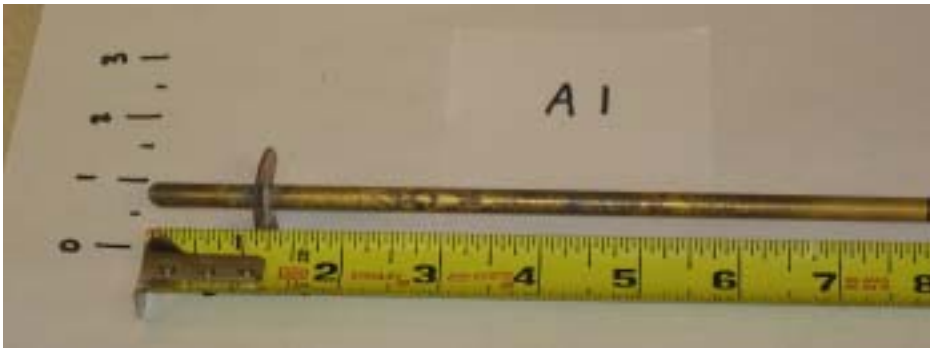
A1


B3


B6

Figure 4.9 Photographs of Excavated Grouted Piers

Physical observations indicated that the significant "finger" like extensions of grout were present at each grouted helical pier. The physical size of these extensions was measured and recorded (L_f) as noted in Table 4.8. In the following discussion, prototype units are used. The range of L_f in prototype was between 38 cm and 133 cm, which was generally between one-third and one-half of the total grout bulb length. The total additional weight of grout bulb placed at each pier is also estimated, including the finger extensions, to be between 341 - 721 kg in prototype, excluding those below 100 kg, where physical problems with installation were noted. The cement in the grout bulb is approximately 20 - 40% of the total weight of the cement in the grout placed in the grout chamber, indicating that additional mixing with the sand has contributed to the weight of the final grout bulb. As noted, the loss of grout was observed post spin, to have remained in the chamber.

The maximum grout bulb diameter D_{max} is also recorded and ranged from 14 cm to 81 cm. The low values (D_{max} = 14 and 19 cm) occurred in those cases where physical problems occurred with the installation (the bottom funnel leaking in this case). It is noted the range of D_{max} is approximately 0.8 – 2.0 times the helix diameter. The length of the major grout bulb (less the finger extensions -- noted as L_b) ranged from 67 -191 cm (excluding those with physical installation problems). This range is well within and greater than the length region over which the target simultaneous grouting and torquing of the piers was conducted (76 cm target draw down depth).

Table 4.8 Centrifuge test results for grout installation (prototype scale)

	Pier No.[1]	L_e (m)	P_i [2] (MPa)	P_x (MPa)	Grout Type [3]	Helix Observation	W_g (kg)	Observation after Excavation [4] (cm)						Possible Explanation
								D_{max}	D_{min}	L_m	L_b	L_f	L	
1st Spin	**A1**	3.8	0.101	0.16	A	helix failed	0	0	0	0	0	0	0	Helix failed & tube leaked.
	A2	3.8	0.101	0.16	A	embedded in grout	570.7	71	48	24	76	130	206	
	A3	5.7	0.101	0.19	A	embedded in grout	587.9	76	52	10	76	133	210	
2nd Spin	**B1**	3.8	0.101	0.16	B	embedded in grout	341.2	46	38	38	126	122	248	
	B2	3.8	0.101	0.16	B	embedded in grout	402.3	48	29	10	191	84	274	
	B3	3.8	0.171	0.23	B	helix failed	0	0	0	0	0	0	0	Helix failed.
3rd Spin	**B4**	3.8	0.171	0.23	B	embedded in grout	559.2	69	45	14	110	69	179	
	B5	5.7	0.101	0.19	B	outside the bulb	548.8	67	48	0	69	122	191	
	B6	5.7	0.101	0.19	B	helix failed	0	0	0	0	0	0	0	Helix failed.

	Pier No.[1]	L_e (m)	P_i [2] (Mpa)	P_x (MPa)	Grout Type [3]	Helix Observation	Wg (kg)	Observation after Excavation (cm)						Possible Explanations
								Dmax	Dmin	Lm	Lb	Lf	L	
1st Spin	C1(*)	3.8	0.101	0.16	A	outside the bulb	47.3	33	29	0	19	38	57	
2nd Spin	D1(*)	3.8	0.171	0.23	B	embedded in grout	721.6	81	67	10	76	122	198	
3rd Spin	D2(*)	3.8	0.101	0.16	B	outside the bulb	28.4	29	19	0	19	38	57	
6th Spin	G1	3.8	0.101	0.16	C	outside the bulb	58.1	14	10	0	30	0	30	Bottom funnel leaked.
	G2	3.8	0.171	0.30	C	helix failed	0.0	0	0	0	0	0	0	Helix failed.
	G3	5.7	0.101	0.19	D	Outside the bulb	81.3	19	11	0	38	0	38	Bottom funnel leaked.

Note: L_e = prototype embedment depth; P_i = grout inject pressure; $P_x = \gamma L_e + P_i$ = total pressure at grout exit hole (γ = soil unit weight: 16.1kN/m^3) W_g = prototype grout bulb weight. All other notations are shown in Figure 3.8.

1. All piers torqued at target 5 rpm, those noted with (*) were installed grout without rotation;
2. 0.101Mpa = atmospheric pressure; 0.101Mpa = 10psi;
3. Table 2.2 gives the grout mix summary;
4. The embedment depth, grout bulb weight and grout bulb dimensions are all in prototype.

4.6 Loading Test Results

As discussed in Section 3.1, three axial loading tests were conducted, with the objective of examining the load improvement when using piers, piers with helices, and grouted helical piers. These loading tests were conducted on the plain pier "E", the helical pier "F", and the grouted helical pier "C1". The measured load-displacement results are plotted in Figures 4.10to 4.12. Similarly, the load-displacement data was low pass filtered in the frequency domain, using a Butterworth filter with a cutoff frequency of 5 Hz. The processing code for this is shown in Appendix A. As stated in Table 3.6, during the loading on the plain pier, the loading block fell off at 0.055 m axial displacement, subsequently, the actuator pushed directly on the top of the pier. Therefore, the curve for the displacement prior to 0.055m axial displacement was extrapolated. The complete curve is plotted in Figure 4.10.

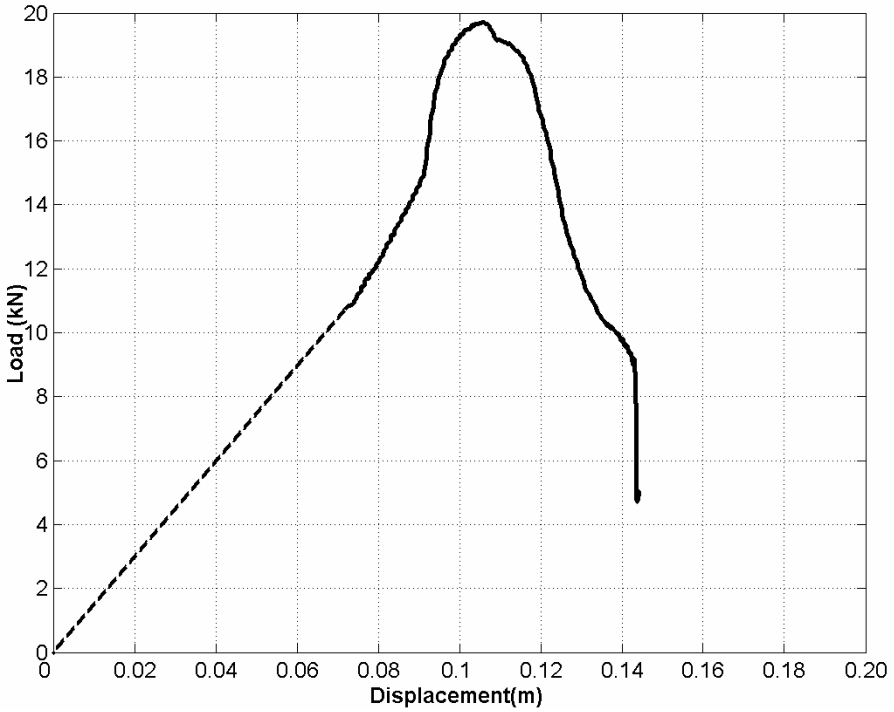

Figure 4.10 Axial load-deflection curve for plain pier "E" loading test (prototype units)

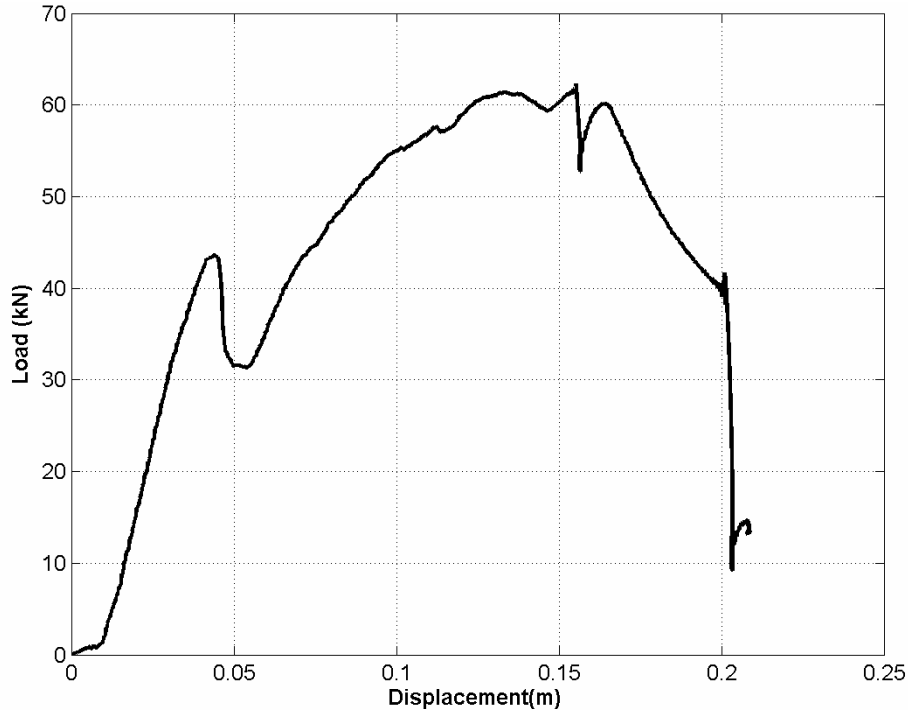

Figure 4.11 Axial load-deflection curve for helical pier "F" loading test (prototype units)

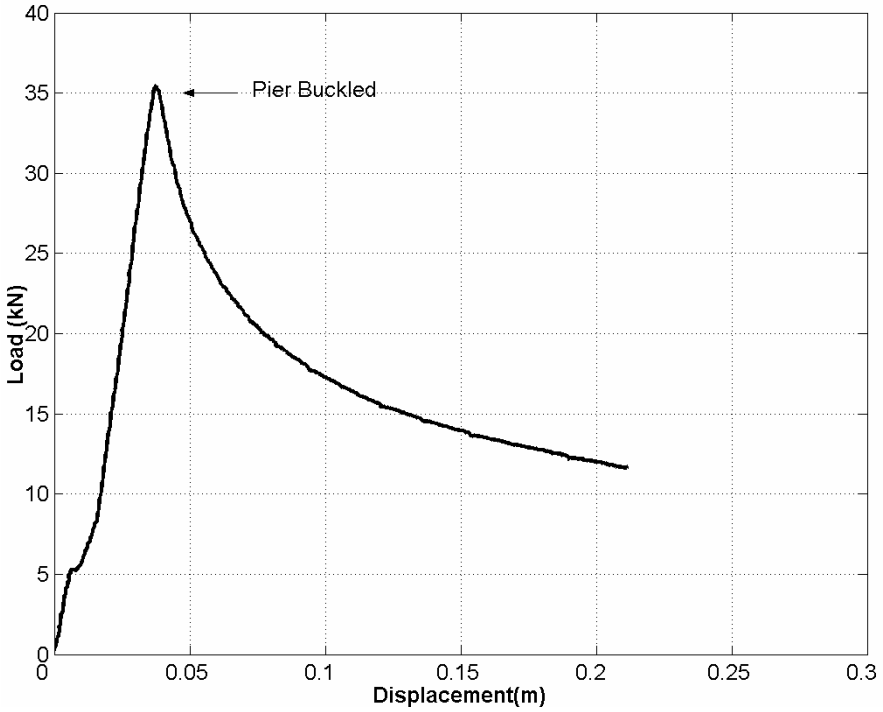

Figure 4.12 Axial load-deflection curve for grouted pier "C1" loading test (prototype units)

For the plain pier at pier location “E”, the pier reached its peak strength of 19.5 kN at an axial displacement of 0.11 m resulting in a secant axial stiffness (at peak) of 177 kN/m. Whereas, the helical pier at the pier location “F” had approximately three times the axial load capacity of 60 kN at 0.12 m displacement, resulting in a secant axial stiffness (at peak) of 500 kN/m. The measured load and stiffness increase can be attributed to the additional bearing resistance provided below the helix. In Figure 4.12, grouted pier “C1” buckled at an axial displacement of 0.03 m and axial load of 35 kN. It is noted that this pier was not originally intended to be loaded axially, thus it was not laterally strengthened above ground. However, the secant (axial) stiffness is 1167 kN/m, more than twice that of the ungrouted helical pier and 6.5 times that of the plain pier. This increase may be attributed to the frictional and bearing resistance provided by the grout bulb.

REFERENCES

A.B. Chance Co. (1991). “Foundation and underpinning system.” BuyLine 1386, A.B. Chance Co., Centralia, MO. (http://www.abchance.com/)

ASTM C939 (1987). “Standard test method for flow of grout for preplaced aggregate concrete (flow cone method).” Annual Book of ASTM Standards, Vol. 04.02.

ASTM D4254 (2000). “Standard test methods for minimum index density and unit weight of soils and calculation of relative density.” Annual Book of ASTM Standards, Vol. 04.08.

ASTM D4253 (2000). “Standard test methods for maximum index density and unit weight of soils using a vibratory table.” Annual Book of ASTM Standards, Vol. 04.08.

Bian, Y. Development and Testing of Centrifuge Tools for Use in Grouted Helical Pier based Foundation Rehabilitation Studies, Masters Thesis, University of California, Irvine. 2006.

Brandenberg, S.J. (2006). Personal communication. Bender system layout.

Brandenberg, S.J., Choie, S., Kutter, B.L., Santamarina, J.C., Wilson, D. (2006). “A bender element system for measuring shear wave velocities in centrifuge models.” Physical Modleing in Geotechnics – 6th ICPMG – Ng, Zhang & Wang (eds), 165p.

Kulhawy, F.H. and Mayne, P.W. (1991). "Manual on estimating soil properties for foundation design." Report EL-6800, Electric Power Research Inst., Palo Alto, 306 p.

Kutter, B.L. (1992). “Dynamic centrifuge modeling of geotechnical structures.” Proceedings of the Transportation Research Record 1336, TRB, National Research Council, Washington, D.C., pp. 24-30.

Laefer D.F., Menninger, N.E. and Hernandez, W.E. (May, 2005). “Grouting patterns and possibilities with helical piers.” Underground Construction in Urban Environments, A Specialty Seminar Presented by ASCE Metropolitan Section Geotechnical Group and the Geo-Institute of ASCE, New York City.

Manke, J.P. (2000). “Assessment of superposition as a design framework for the combined effects of soil improvement and foundation remediation.” Master’s Thesis, North Carolina State University, 221 p.

Meyerhof, G.G. (1956). “Penetration tests and bearing capacity of cohesionless soils.” Journal of the soil Mechanics and Foundation Division, ASCE, vol. 82, No. SM1, pp. 1-19.

NEES@UCDAVIS, Retrieved May, 2006, from: http://nees.ucdavis.edu/.

Nittetsu Cement Co., Retrieved June, 2006, from: http://www.nittetsu-cement.co.jp/.

Nichols, S.C. and Goodings, D.J. (2000). “Physical model testing of compaction grouting in cohesionless soil.” Journal of Geotechnical and Geoenvironmental Engineering, Vol. 126, No.9, pp. 848-852.

Phillips, R. and Valsangkar, A.J. (1987). “An experimental investigation of factors affecting penetration resistance in granular soils in centrifuge modeling.” Report CUED/D-Soils TR 210, Cambridge.

Precision Pier. (Dec, 2005). Personal communication (www.precisionpierusa.com)

Renzi, R. J.F., Corte, G., Bagger, M. Gui, J. Laue (1994). “Cone penetration tests in the centrifuge: experience of five laboratories.” Proc. of International Conference Centrifuge 94, Singapore, September, pp. 77-82.

Robetson, P.K. and Campanella, R.G. (1983). “Interpretation of cone penetration tests. Part I: Sand.” Can. Geotech. J., 20, pp. 718 - 733.

Appendix A: Matlab Calculation Code

A1: Matlab Code for CPT Data Plot

```
load cpt.txt
H = cpt(:, 1:2);

stop = 4096 * 62;
Disp = H(1 : stop, 1);
Load = H(1 : stop, 2);

s_frq = 4096;  % the sampling frequency is 4096 HZ
t = (0 : length(Disp) - 1)' / s_frq;

cutoff = 5;

iDisp = denoise_fft(Disp, s_frq, cutoff);
iLoad = denoise_fft(Load, s_frq, cutoff);

xm = max(iDisp); ix = find(iDisp == xm);
ym = max(iLoad); iy = find(iLoad == ym);

index = min([ix; iy]);
iDisp = iDisp(1 : index); iLoad = iLoad(1 : index);
t = t(1 : index);

fX = 1.52*(iDisp)*15/100;
fY = (1.426*(iLoad-min(iLoad)))*15*15/28.26;

figure;
plot(fY, -fX, 'k-');
xlabel('Cone Tip Resistance (MPa)');
ylabel('Depth (m)'); grid;
```

A2: Matlab Code for Plain Pier Loading Test Data Plot

```
load plain.txt;

H = plain(:, 1:2); clear plain;
stop = 4096 *30;
Disp = H(1 : stop, 1);
Load = H(1 : stop, 2);

Disp = H(:, 1);
Load = H(:, 2);

s_frq = 4096;  % the sampling frequency is 4096 HZ
t = (0 : length(Disp) - 1)' / s_frq;


cutoff = 5;

iDisp = denoise_fft(Disp, s_frq, cutoff);
iLoad = denoise_fft(Load, s_frq, cutoff);


% plain pier
Dx = (iDisp-0.836) * 15.22 *15*0.001;  %(m)
Dy = (iLoad-0.037) * 242.9 * 15* 15/(10^3);  %(kN)

% figure;
% plot(t,Dx);
% ylabel('Displacement(m)'); xlabel('time(sec)');
% grid;

N = length(Dx);
X = Dx(48000:N);
Y = Dy(48000:N);

figure % , plot(iDisp, iLoad, 'r.'); hold on;
plot(X,Y, 'k-');
xlabel('Displacement(m)'); ylabel('Load (kN)');
grid;
```

A3: Matlab Code for Plain Pier Loading Test Data Plot

```
load helical.txt;

H = helical(:, 1:2); clear helical;
stop = 4096 * 110;
Disp = H(1 : stop, 1);
Load = H(1 : stop, 2);


s_frq = 4096;  % the sampling frequency is 4096 HZ

t = (0 : length(Disp) - 1)' / s_frq;

%  the noisy orignial plot
figure, plot(Disp, Load, '.');
xlabel('Disp'); ylabel('Loads');
grid;


cutoff = 5;

iDisp = denoise_fft(Disp, s_frq, cutoff);
iLoad = denoise_fft(Load, s_frq, cutoff);


% helical pier
Dx = (iDisp-0.0182) * 15.22 *15*0.001;  %(m)
Dy = (iLoad-0.14) * 242.9 * 15* 15/(10^3);  %(kN)


N = length(Dx);
X = Dx(201800:N)-0.19;
Y = Dy(201800:N);

figure % , plot(iDisp, iLoad, 'r.'); hold on;
plot(X, Y, 'k-');
xlabel('Displacement(m)');
ylabel('Load (kN)'); grid;
```

A4: Matlab Code for Grouted Helical Pier Loading Test Data Plot

```
load grouted.txt;

H = grouted(:, 1:2); clear helical;
stop = 4096 * 52;
Disp = H(1 : stop, 1);
Load = H(1 : stop, 2);


s_frq = 4096;  % the sampling frequency is 4096 HZ
t = (0 : length(Disp) - 1)' / s_frq;

%  the noisy orignial plot
figure, plot(Disp, Load, '.');
xlabel('Disp'); ylabel('Loads');
grid;


cutoff = 5;

iDisp = denoise_fft(Disp, s_frq, cutoff);
iLoad = denoise_fft(Load, s_frq, cutoff);


%grouted helical pier
Dx = (iDisp) * 15.22 *15*0.001;  %(m)
Dy = (iLoad+4.34) * 242.9 *15 *15/1000;  %(kN)

N = length(Dx);
X = Dx(34000:N)-0.14;
Y = Dy(34000:N);

figure;
plot(X, Y, 'k-');
xlabel('Displacement(m)'); ylabel('Load (kN)');
grid;
```

Appendix B: Additional Photographs of Observed Grouted Helical Piers

B1. Additional Photos of the Grouted Helical Piers during the Excavation


c1


D2

B2. Overview of Excavated Grouted Helical Pier Photos

Appendix C: Bender Data Plots

The bender data plotted below was collected using LabView software written by Scott Brandenberg and Seokhyeon Choi, and hardware housed on the RESDAQ-AUX computer.

C1 Plots for bender data collected at 15-g before grouting

Plots from data file "YYB0106082006143915.txt"

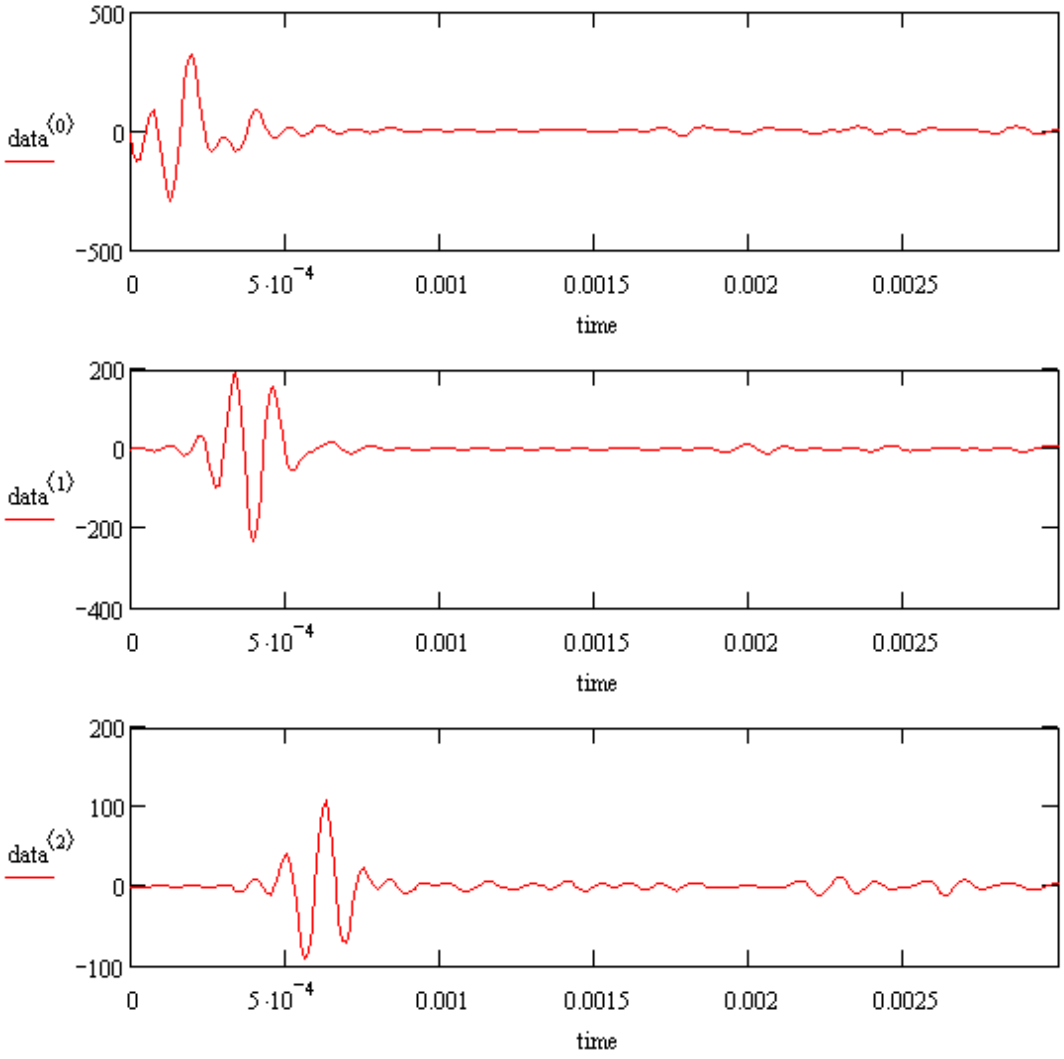

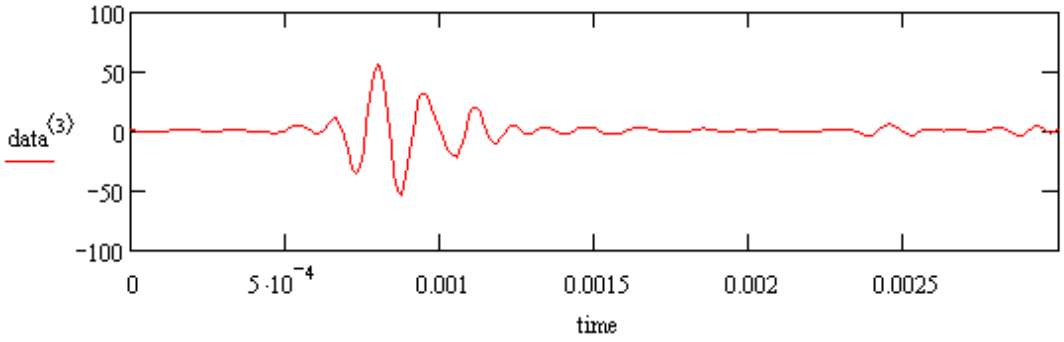
data(3)
100
50
0
−50
−100
0
5·10^−4
0.001
0.0015
0.002
0.0025
time

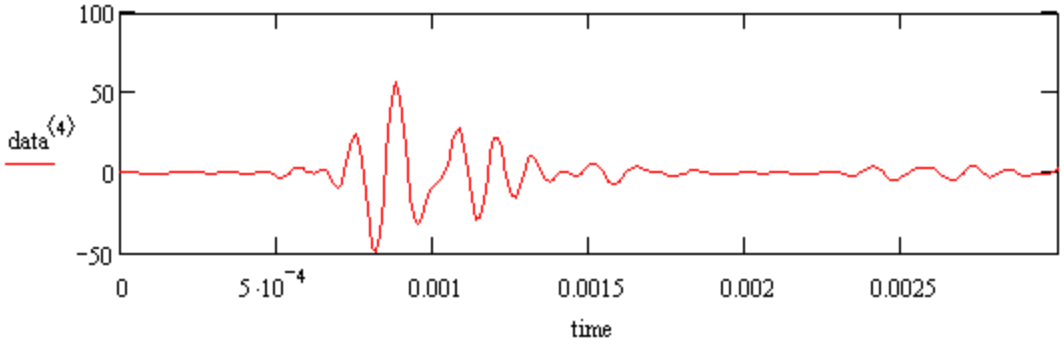
data(4)
100
50
0
−50
0
5·10^−4
0.001
0.0015
0.002
0.0025
time

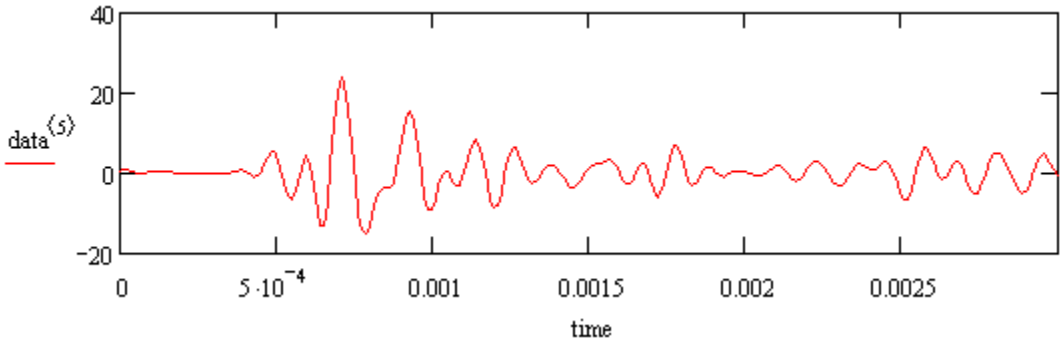
data(5)
40
20
0
−20
0
5·10^−4
0.001
0.0015
0.002
0.0025
time

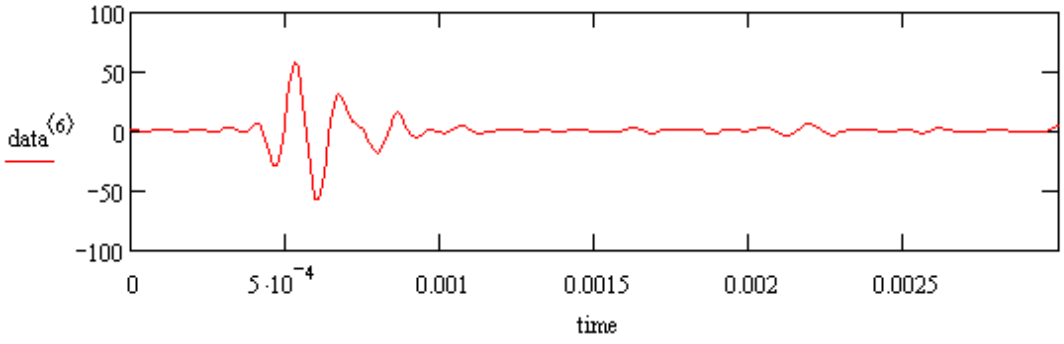
data(6)
100
50
0
−50
−100
0
5·10^−4
0.001
0.0015
0.002
0.0025
time

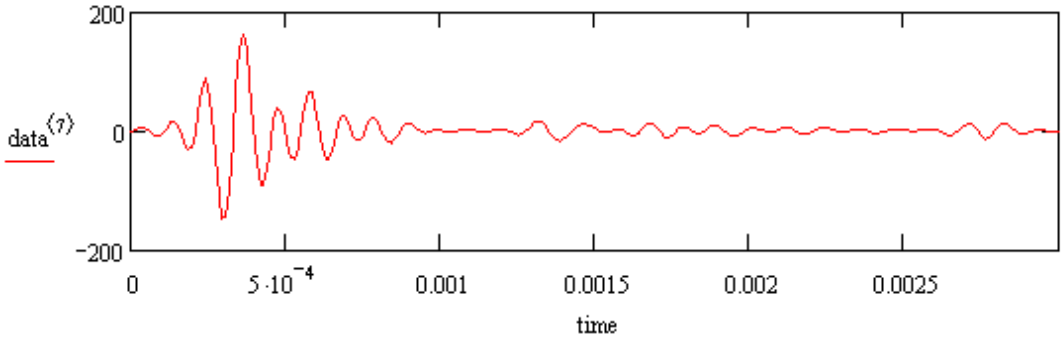

Plots from data file “YYB0106082006143920.txt”

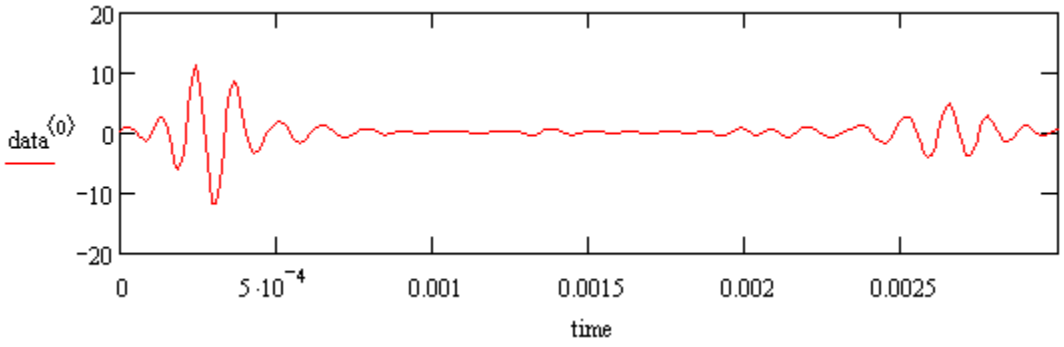

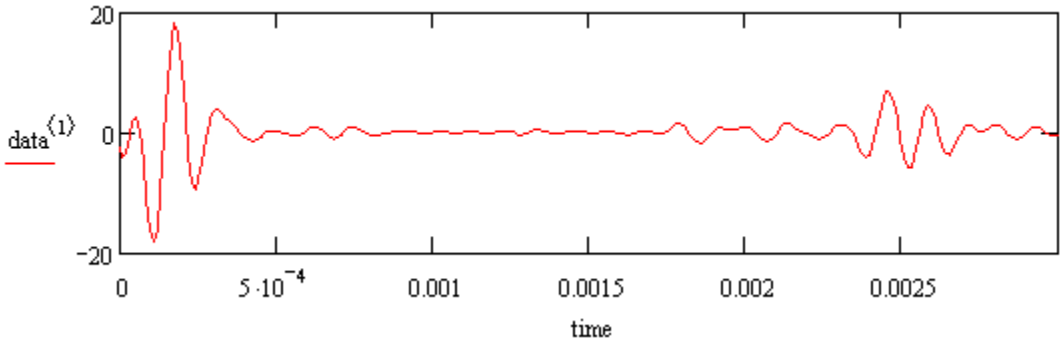

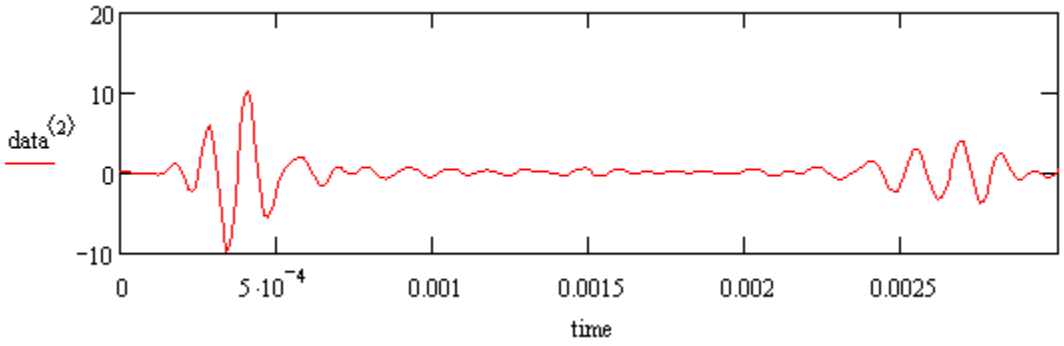

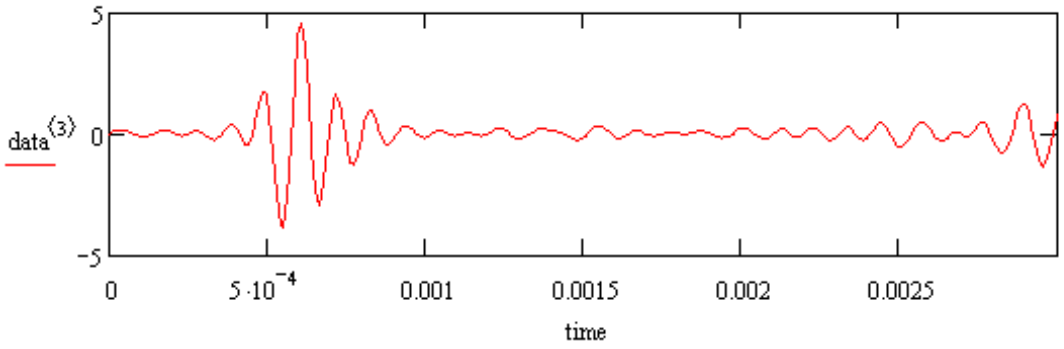
data⟨3⟩
5
0
−5
0
5·10^−4
0.001
0.0015
0.002
0.0025
time

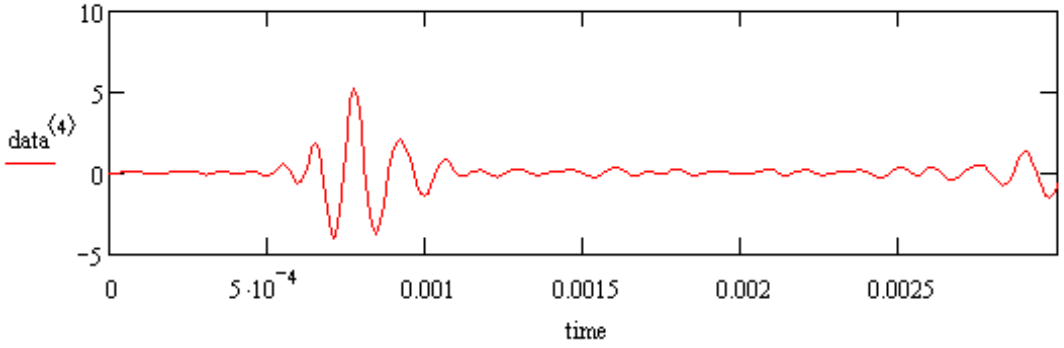
data⟨4⟩
10
5
0
−5
0
5·10^−4
0.001
0.0015
0.002
0.0025
time

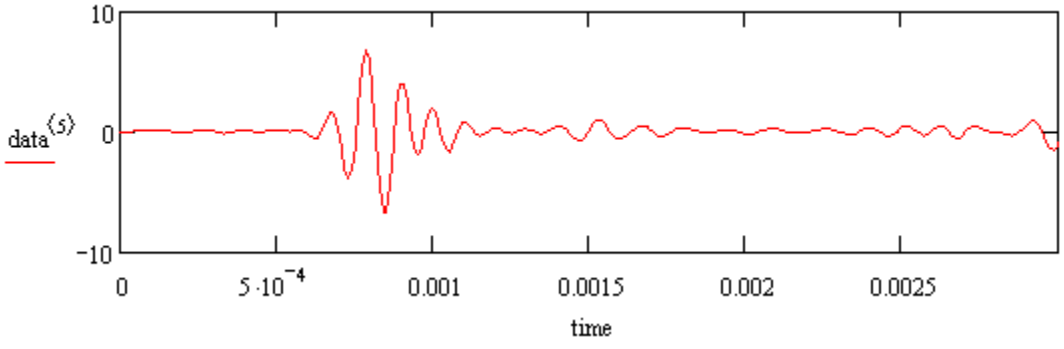
data⟨5⟩
10
0
−10
0
5·10^−4
0.001
0.0015
0.002
0.0025
time

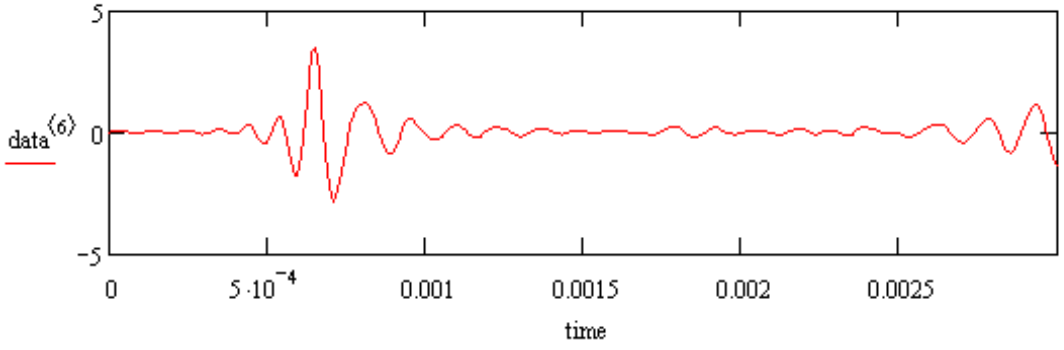
data⟨6⟩
5
0
−5
0
5·10^−4
0.001
0.0015
0.002
0.0025
time

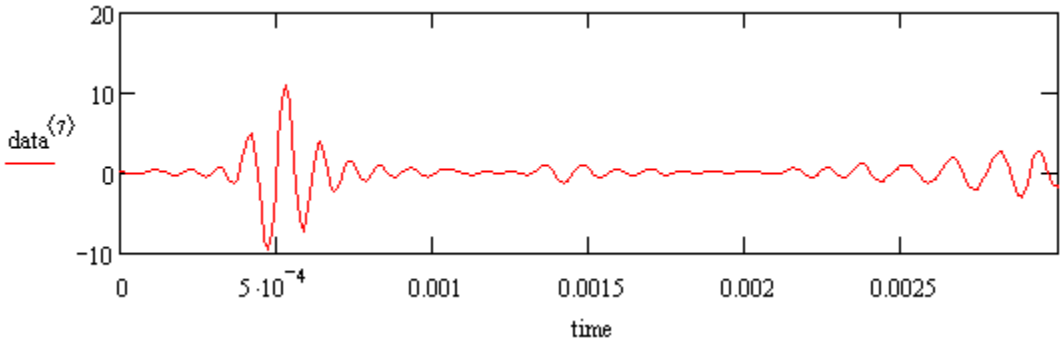

Plots from data file “YYB0106082006143921.txt”

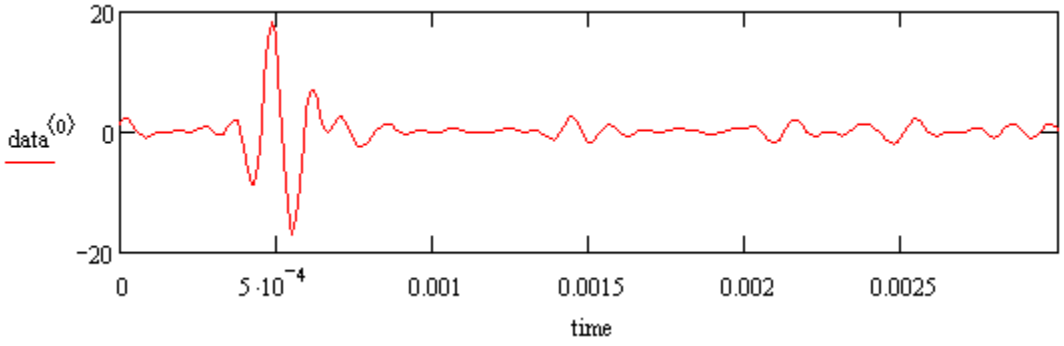

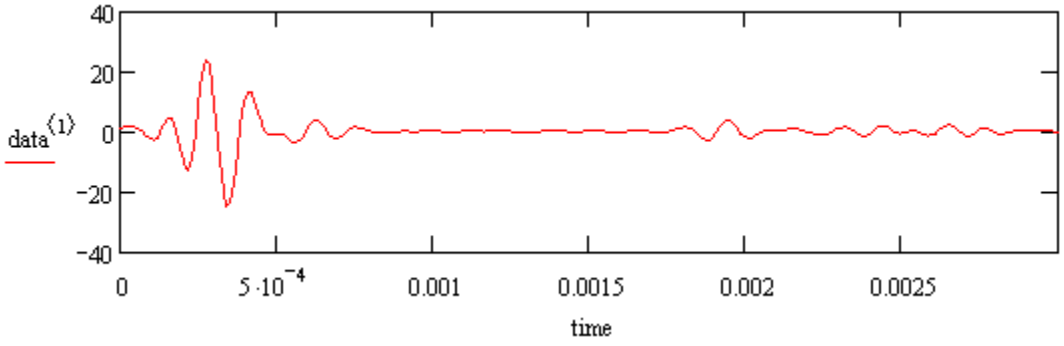

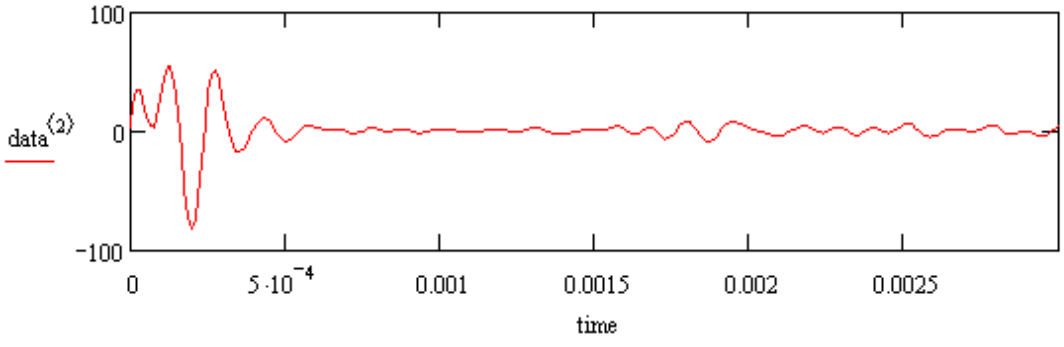

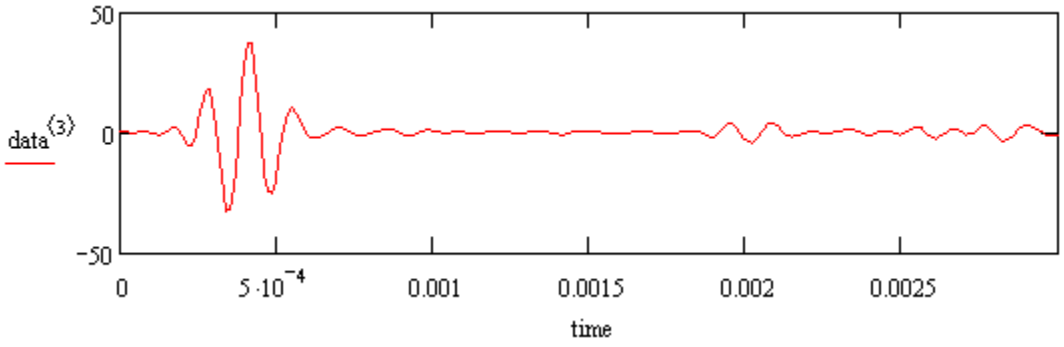
data⟨3⟩
50
0
−50
0
5·10^−4
0.001
0.0015
0.002
0.0025
time

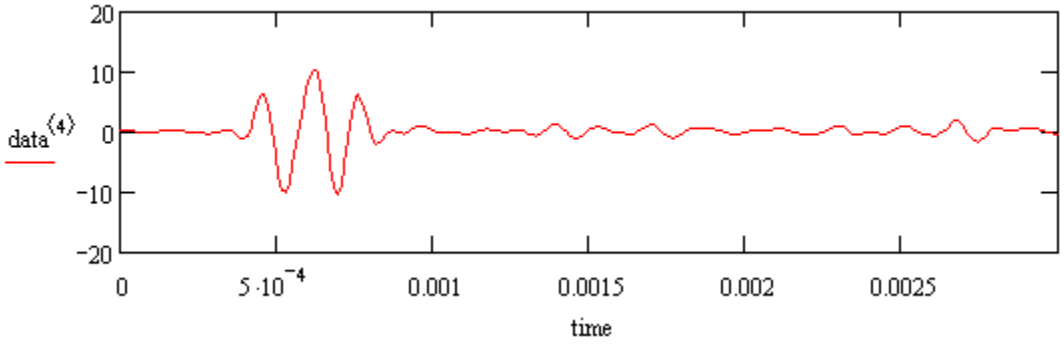
data⟨4⟩
20
10
0
−10
−20
0
5·10^−4
0.001
0.0015
0.002
0.0025
time

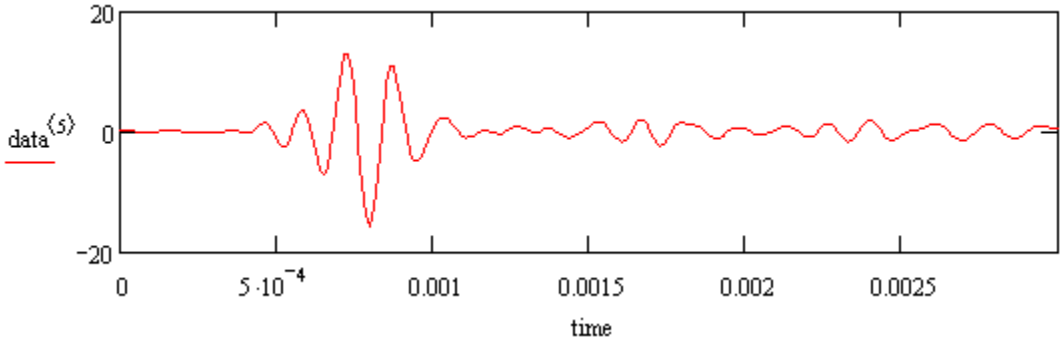
data⟨5⟩
20
0
−20
0
5·10^−4
0.001
0.0015
0.002
0.0025
time

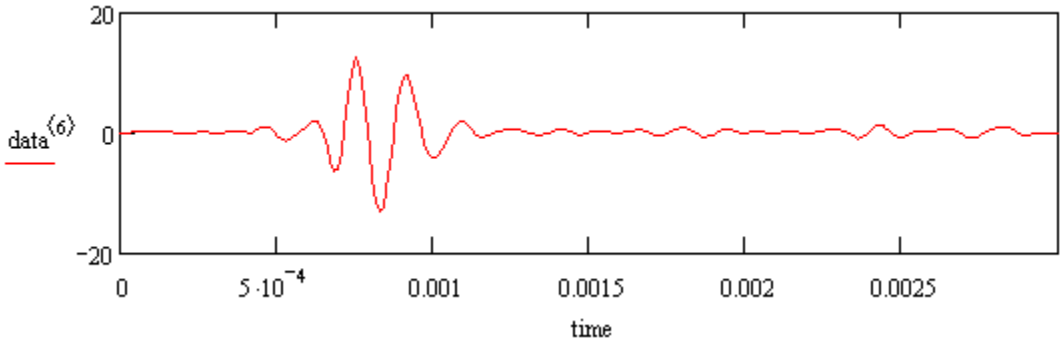
data⟨6⟩
20
0
−20
0
5·10^−4
0.001
0.0015
0.002
0.0025
time

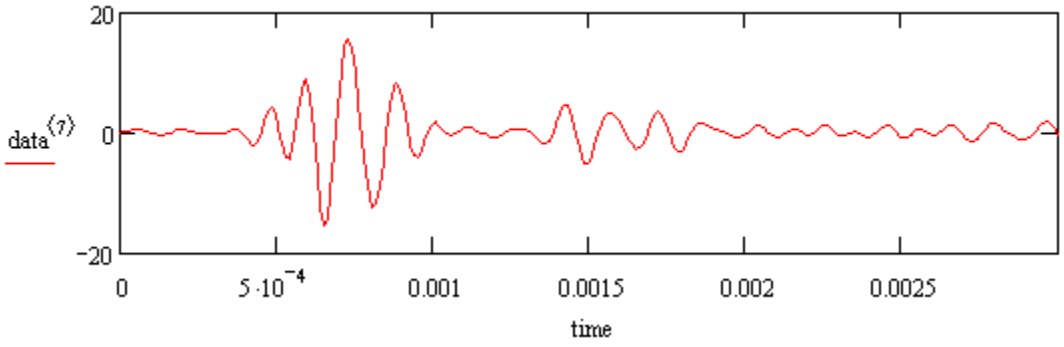

Plots from data file “YYB0106082006143923.txt”

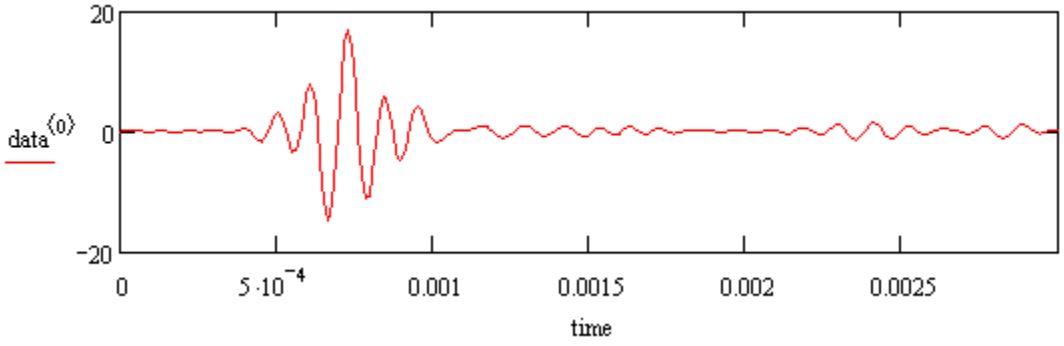

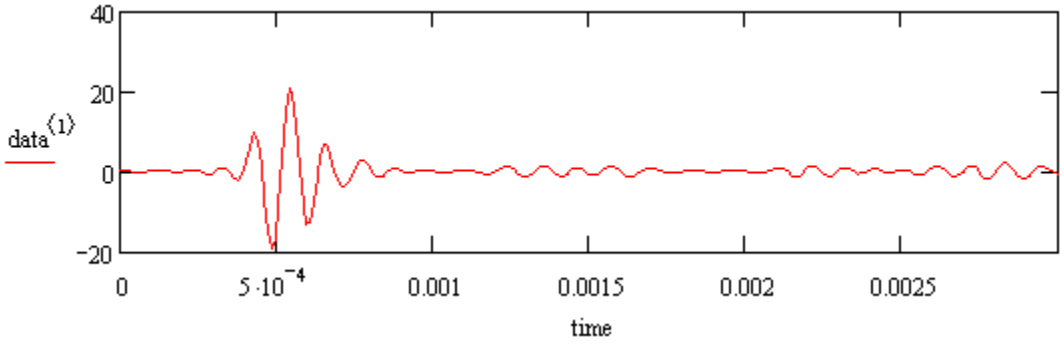

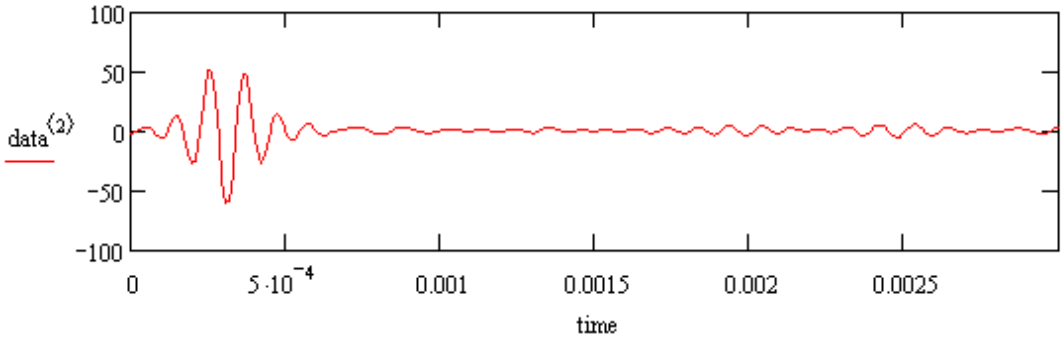

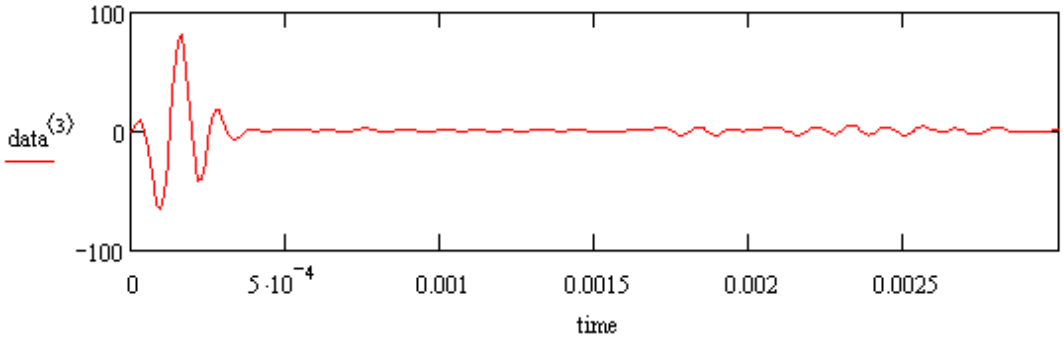
100
0
−100
data⟨3⟩
0
5·10^−4
0.001
0.0015
0.002
0.0025
time

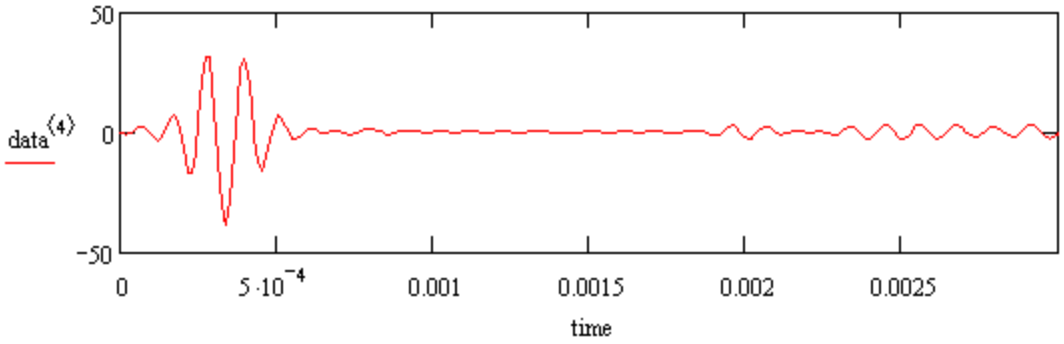
50
0
−50
data⟨4⟩
0
5·10^−4
0.001
0.0015
0.002
0.0025
time

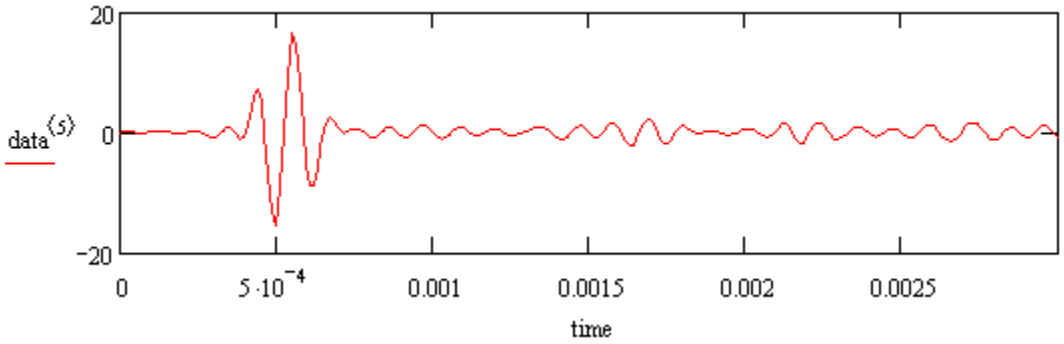
20
0
−20
data⟨5⟩
0
5·10^−4
0.001
0.0015
0.002
0.0025
time

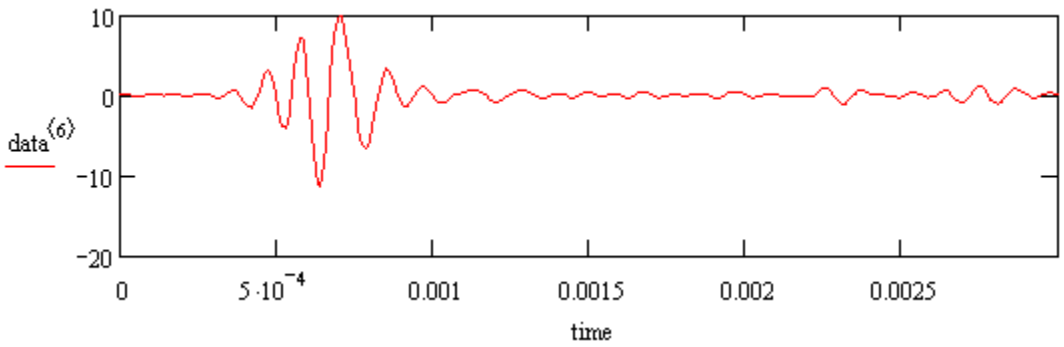
10
0
−10
−20
data⟨6⟩
0
5·10^−4
0.001
0.0015
0.002
0.0025
time

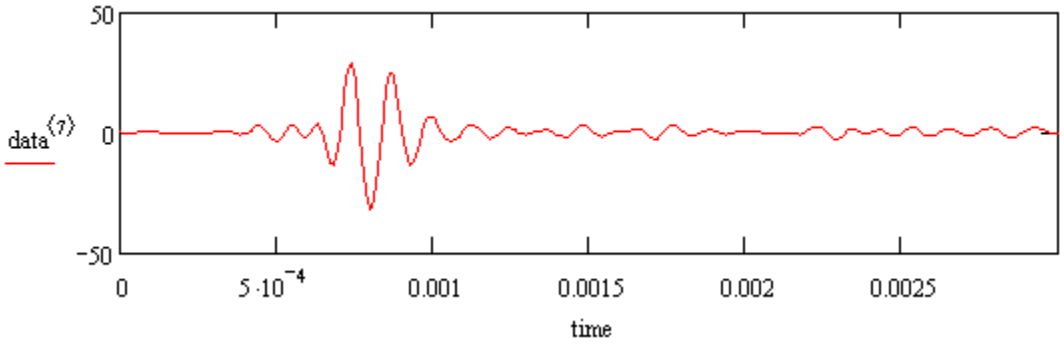

C2 Plots for bender data collected at 15-g after grouting

Plots from data file “YYB0106132006152837.txt”

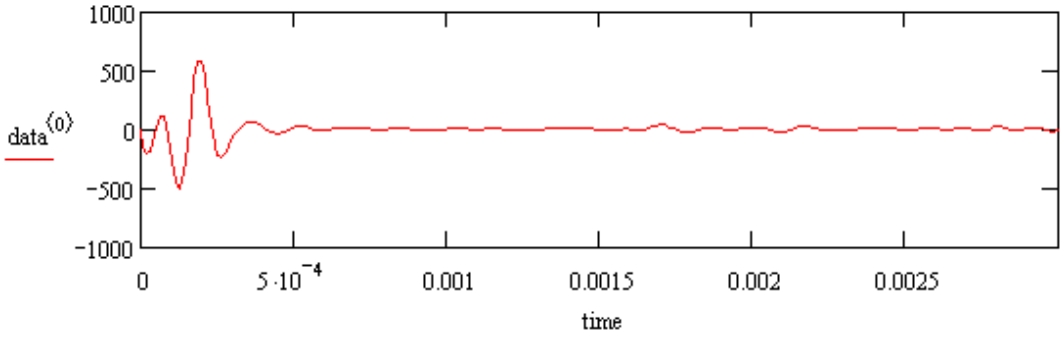

Plots from data file “YYB0106132006152837.txt”

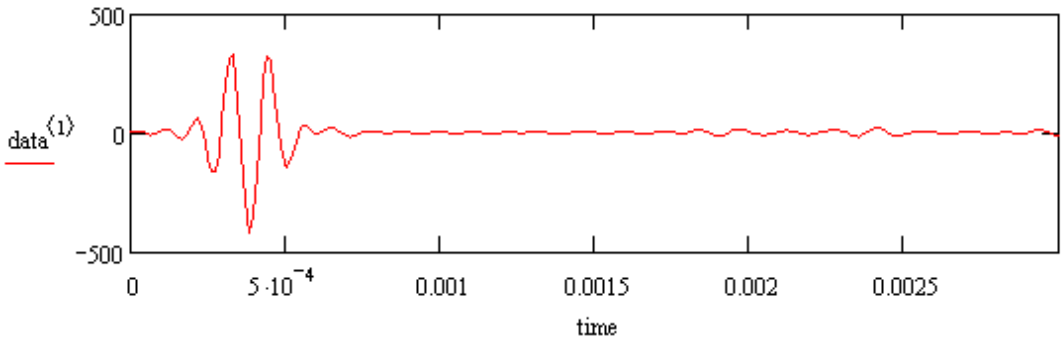

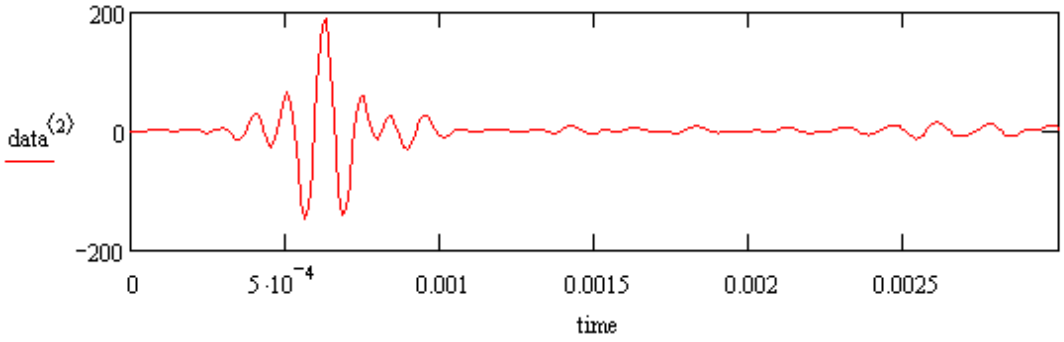
data(2)
200
0
−200
0
5·10^−4
0.001
0.0015
0.002
0.0025
time

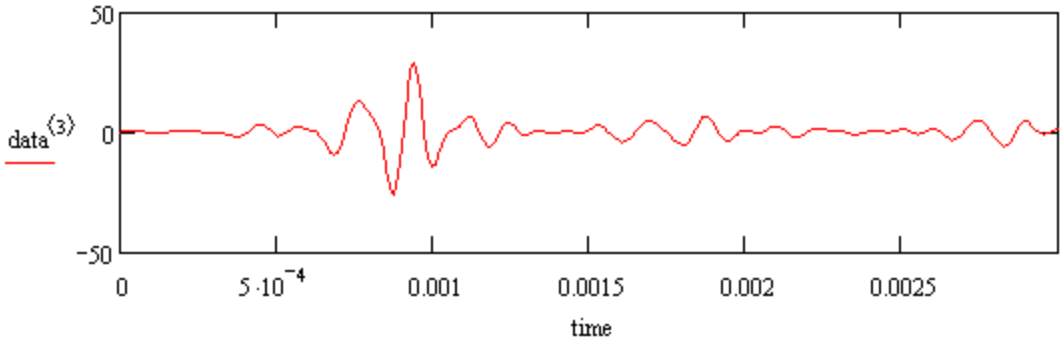
data(3)
50
0
−50
0
5·10^−4
0.001
0.0015
0.002
0.0025
time

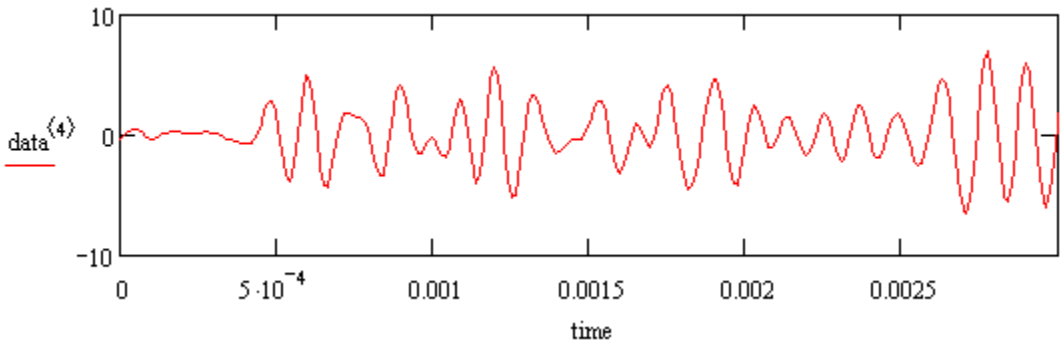
data(4)
10
0
−10
0
5·10^−4
0.001
0.0015
0.002
0.0025
time

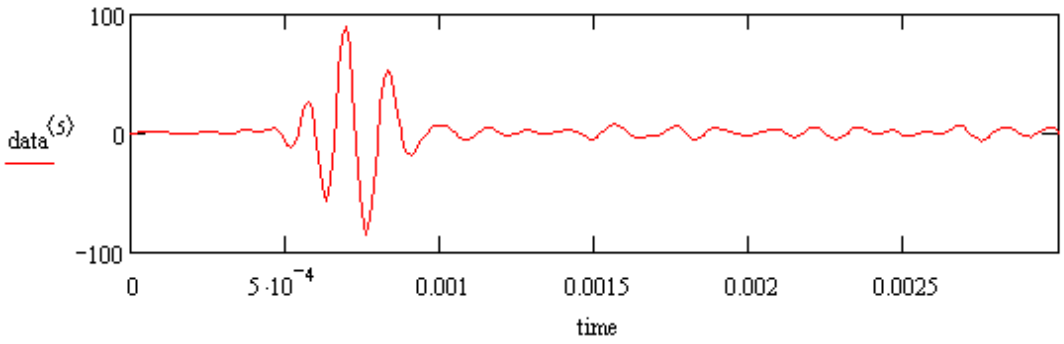
data(5)
100
0
−100
0
5·10^−4
0.001
0.0015
0.002
0.0025
time

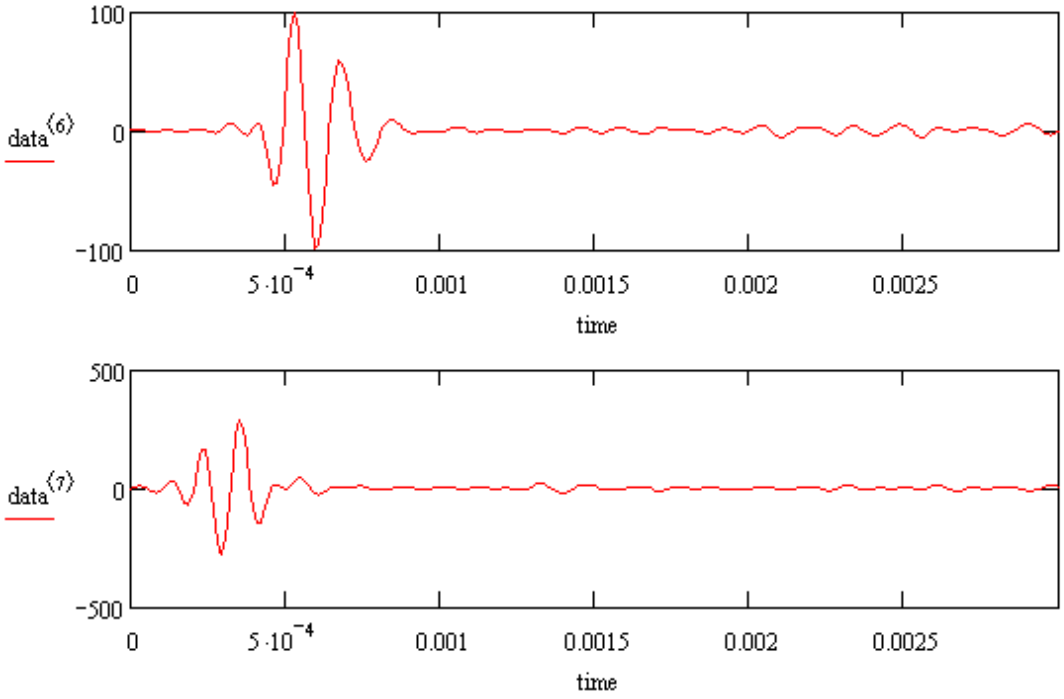

Plots from data file “YYB0106132006152843.txt”

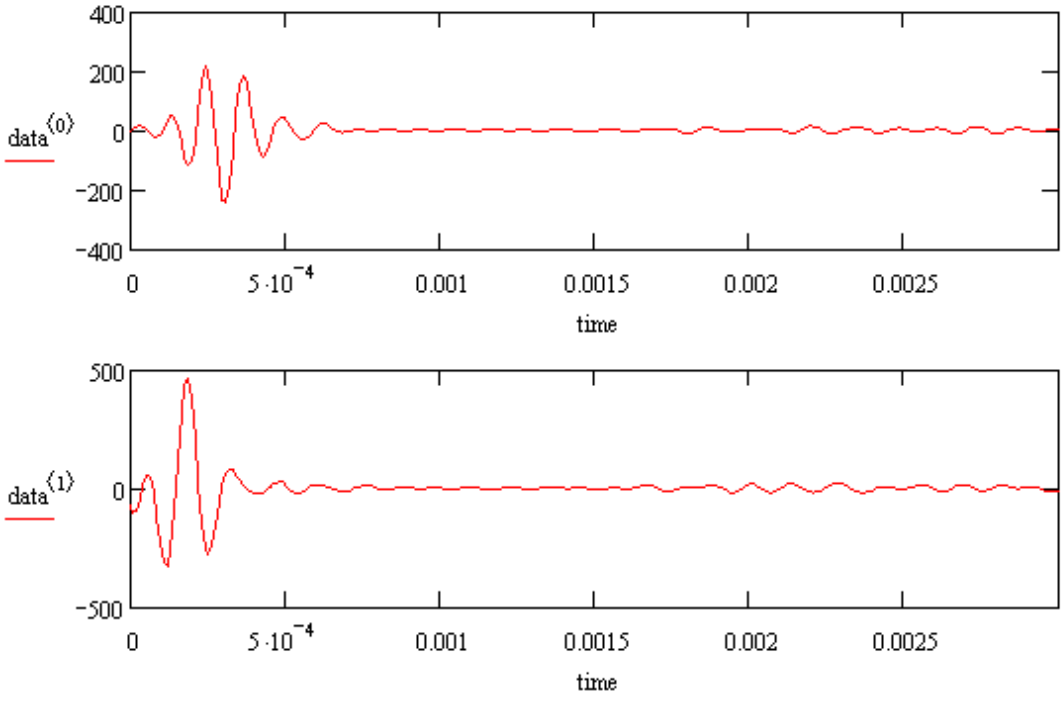

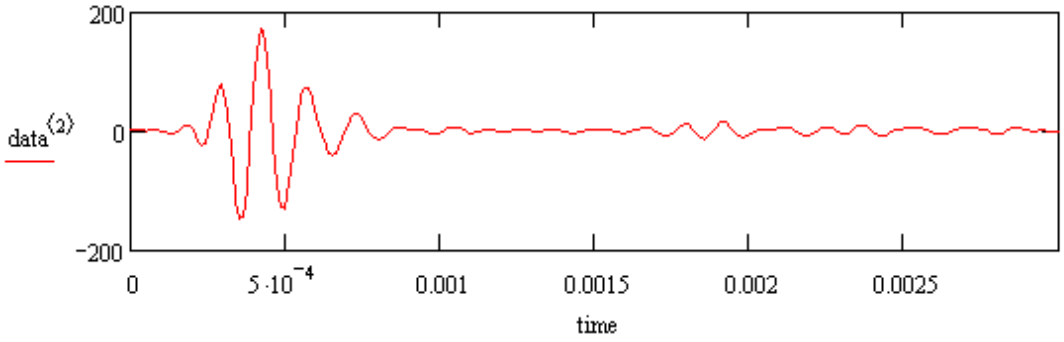
data(2)
200
0
−200
0
5·10^−4
0.001
0.0015
0.002
0.0025
time

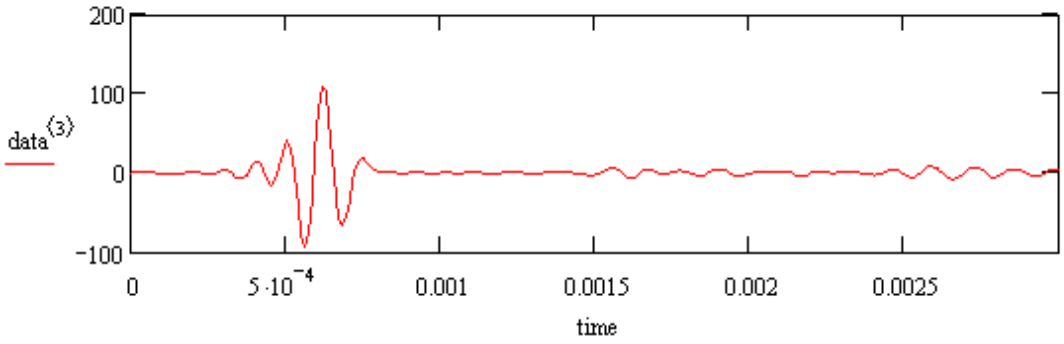
data(3)
200
100
0
−100
0
5·10^−4
0.001
0.0015
0.002
0.0025
time

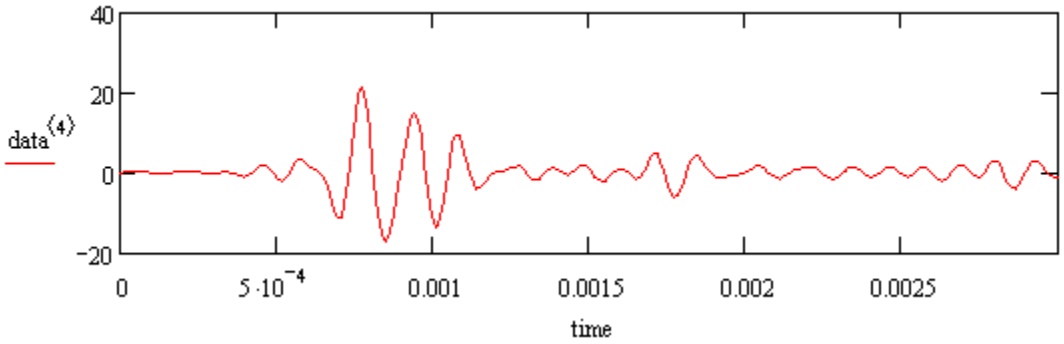
data(4)
40
20
0
−20
0
5·10^−4
0.001
0.0015
0.002
0.0025
time

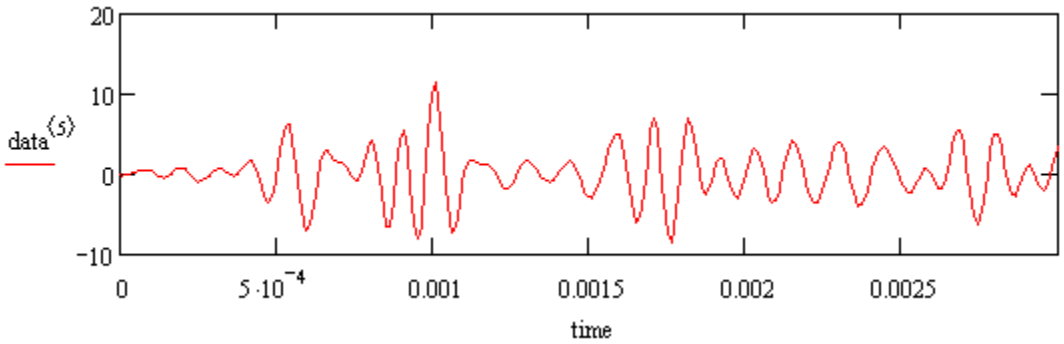
data(5)
20
10
0
−10
0
5·10^−4
0.001
0.0015
0.002
0.0025
time

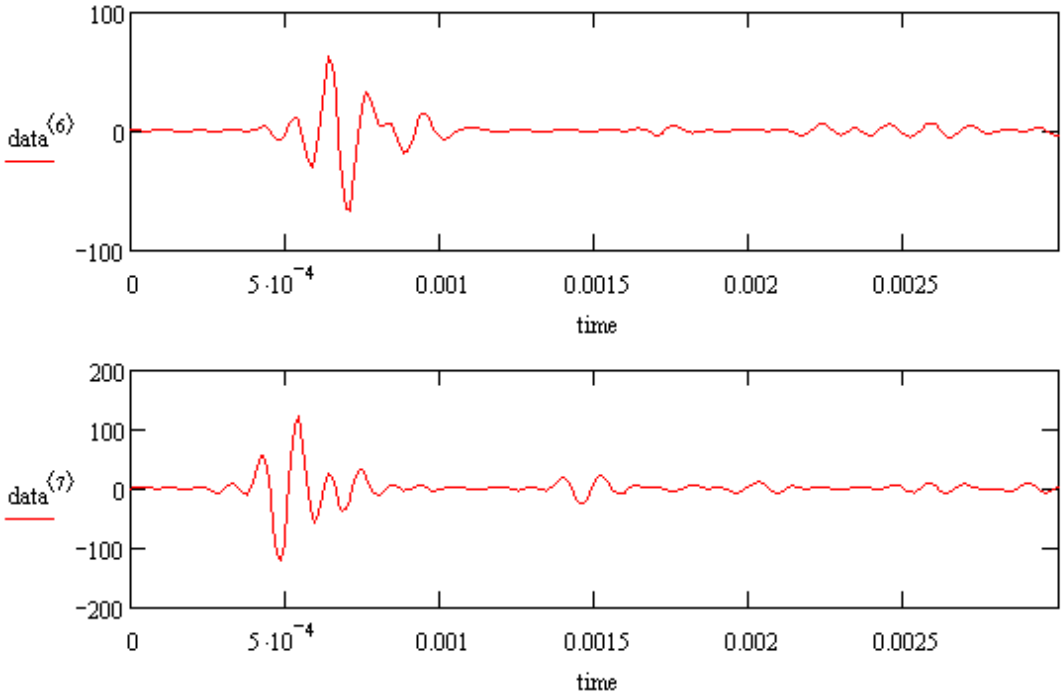

Plots from data file “YYB0106132006152848.txt”

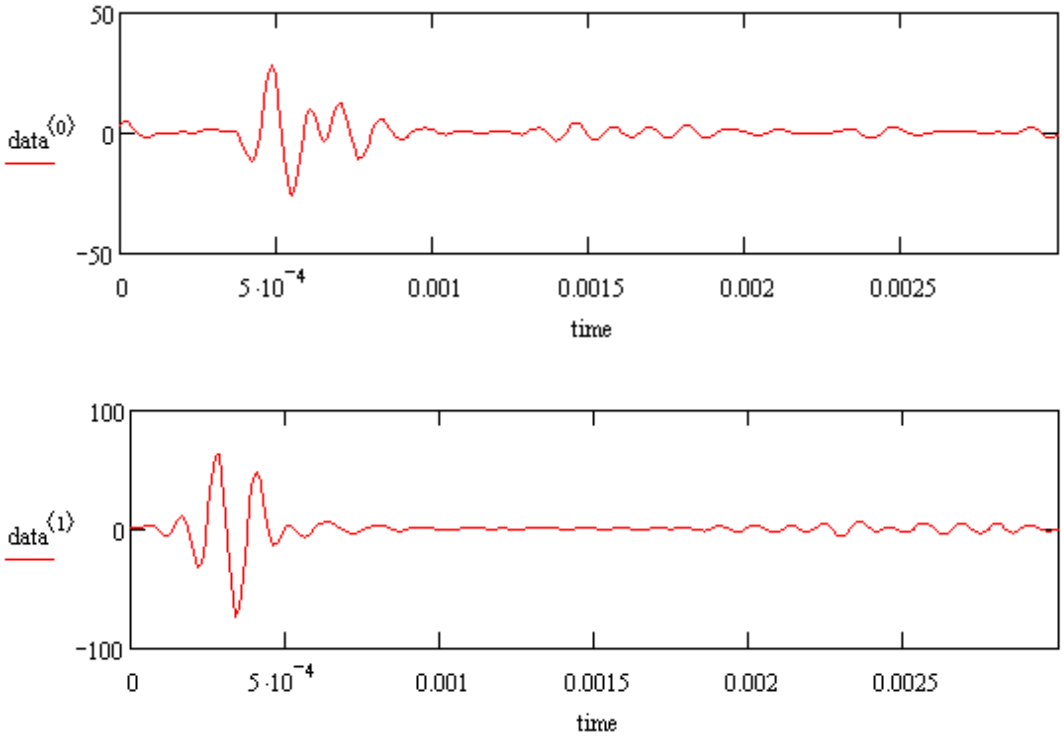

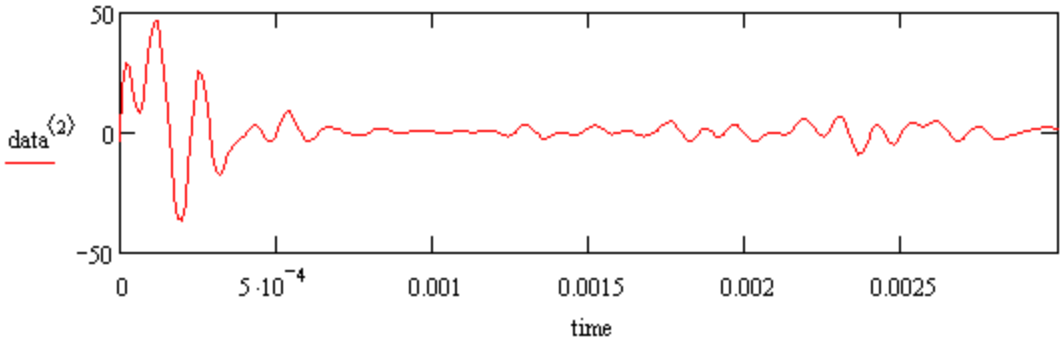
50
0
−50
data⟨2⟩
0
5·10^−4
0.001
0.0015
0.002
0.0025
time

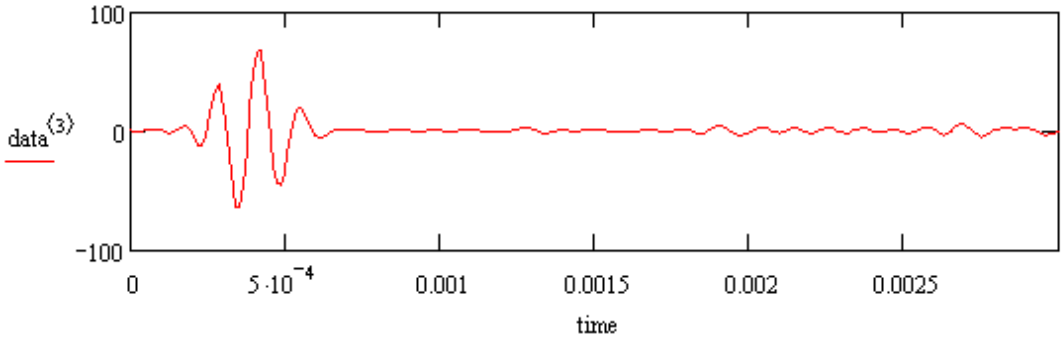
100
0
−100
data⟨3⟩
0
5·10^−4
0.001
0.0015
0.002
0.0025
time

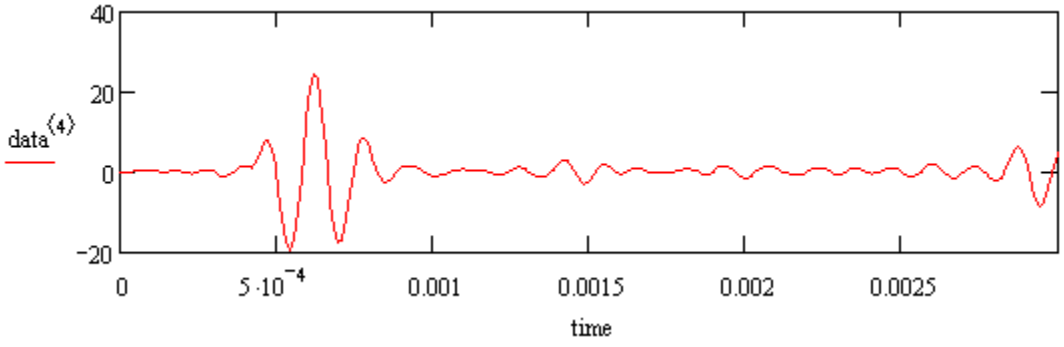
40
20
0
−20
data⟨4⟩
0
5·10^−4
0.001
0.0015
0.002
0.0025
time

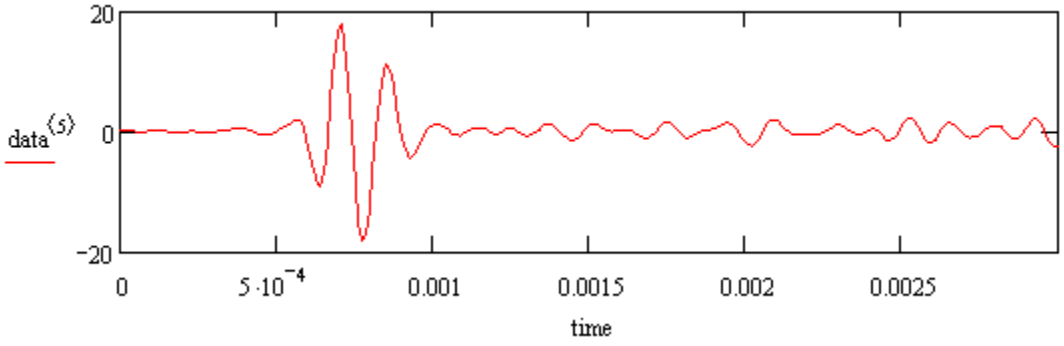
20
0
−20
data⟨5⟩
0
5·10^−4
0.001
0.0015
0.002
0.0025
time

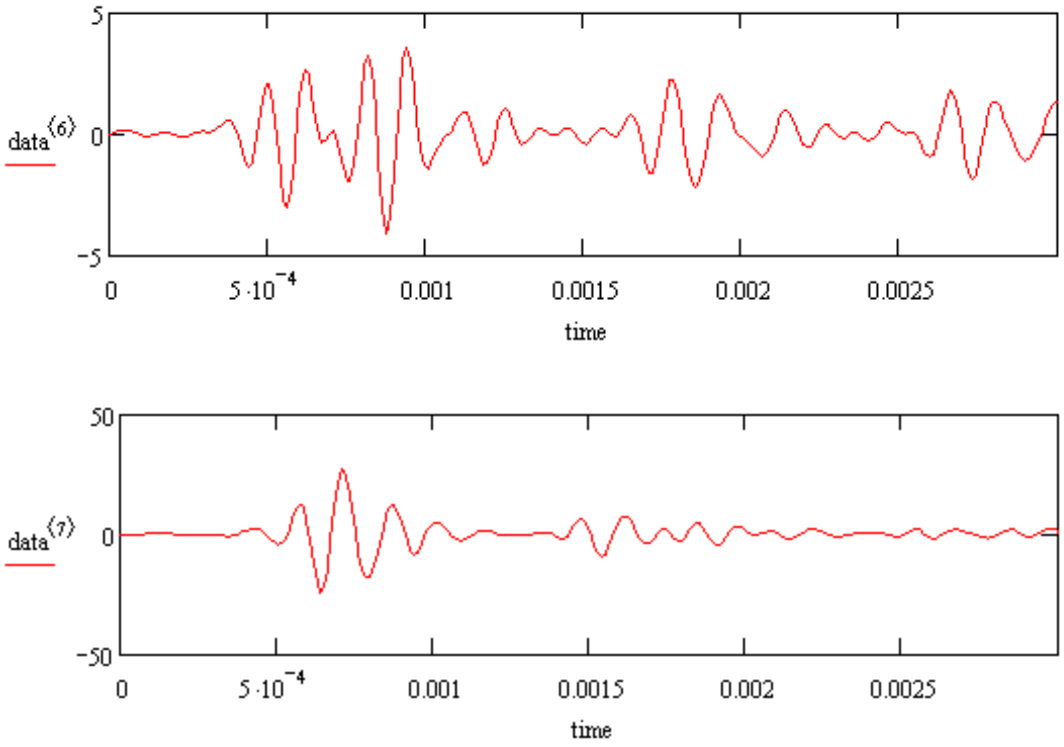

Plots from data file “YYB0106132006152850.txt”

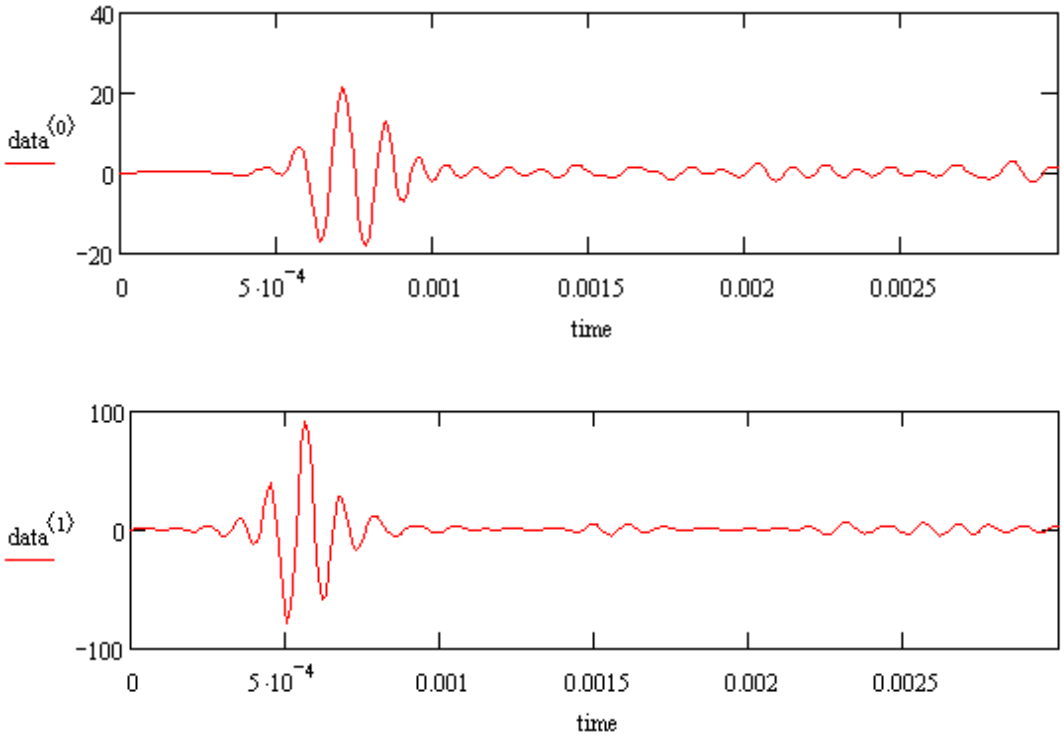

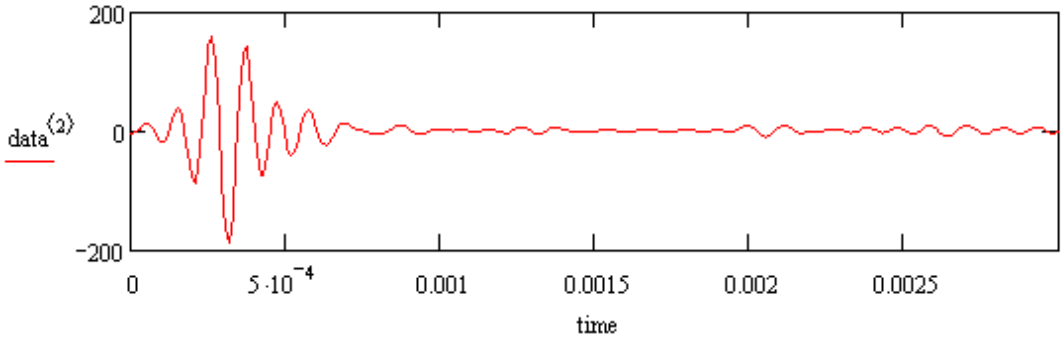
data(2)
200
0
−200
0
5·10^−4
0.001
0.0015
0.002
0.0025
time

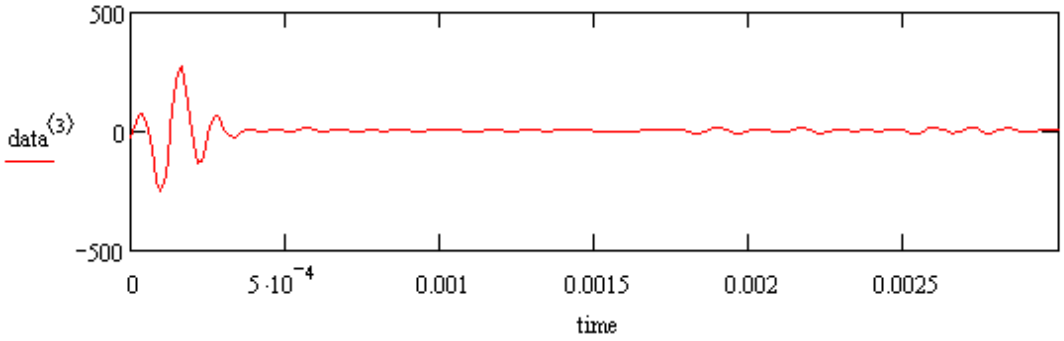
data(3)
500
0
−500
0
5·10^−4
0.001
0.0015
0.002
0.0025
time

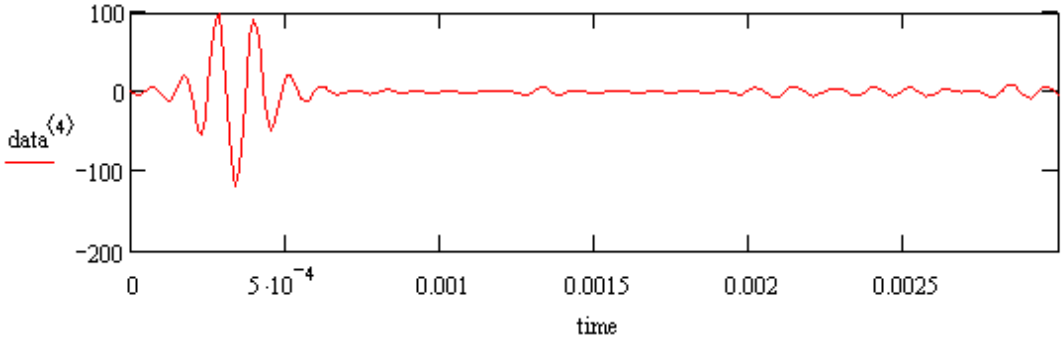
data(4)
100
0
−100
−200
0
5·10^−4
0.001
0.0015
0.002
0.0025
time

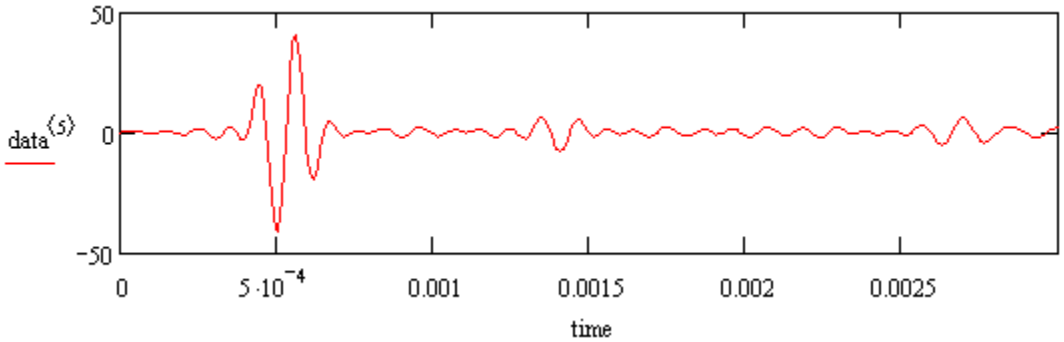
data(5)
50
0
−50
0
5·10^−4
0.001
0.0015
0.002
0.0025
time

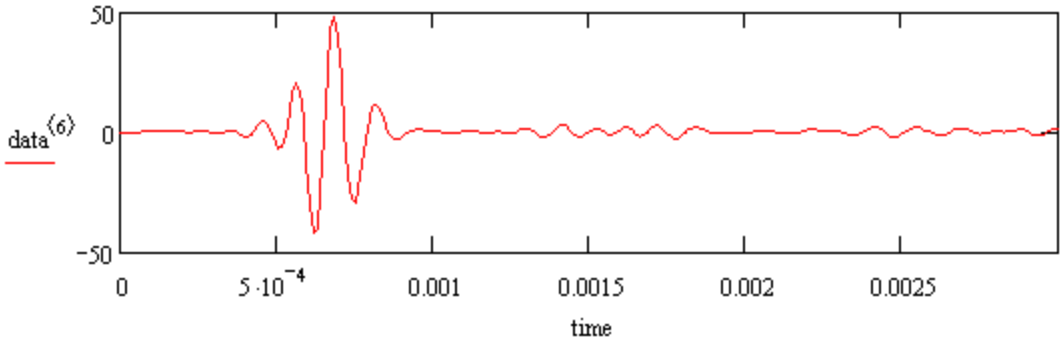
data⟨6⟩
50
0
−50
0
5·10^−4
0.001
0.0015
0.002
0.0025
time

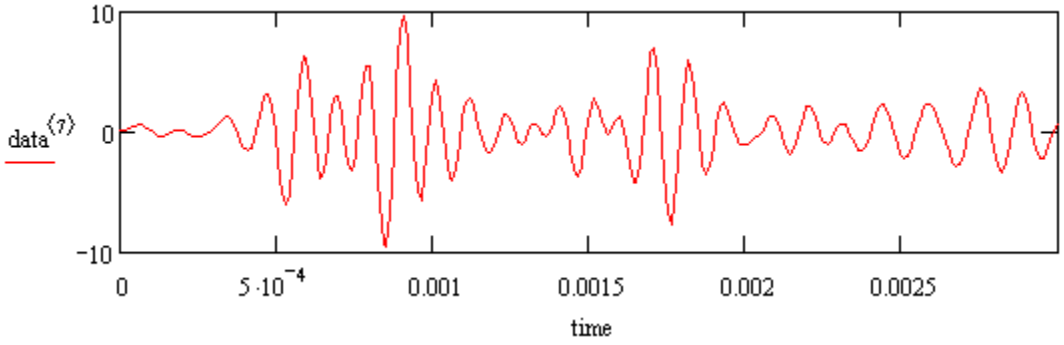
data⟨7⟩
10
0
−10
0
5·10^−4
0.001
0.0015
0.002
0.0025
time